Inorganic Chemistry

Article

pubs.acs.org/IC

Highly Enhanced Bisignate Circular Dichroism of Ferrocene-Bridged Zn(II) Bisporphyrin *Tweezer* with Extended Chiral Substrates due to Well-Matched Host–Guest System

Sanfaori Brahma, Sk Asif Ikbal, Avinash Dhamija, and Sankar Prasad Rath*

Department of Chemistry, Indian Institute of Technology Kanpur, Kanpur-208016, India

Supporting Information

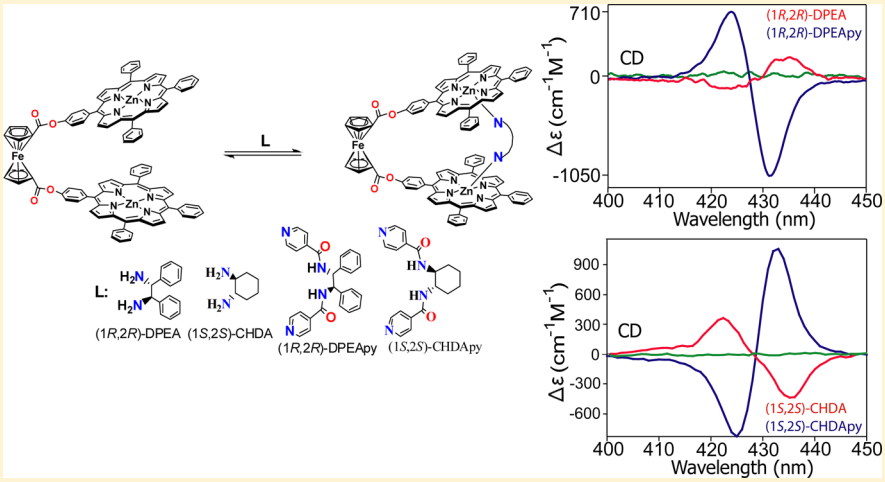

ABSTRACT: Four new chiral *tweezer*-diamine complexes, consisting of an achiral ferrocene-bridged Zn(II)bisporhyrin host (**1**) and two small diamines (1*R*,2*R*)-1,2-diphenylethylene diamine {(1*R*,2*R*)-DPEA} and (1*S*,2*S*)-1,2-cyclohexane diamine {(1*S*,2*S*)-CHDA} and two extended diamines (1*R*,2*R*)-*N*,*N*′-bis-(isonicotinoyl)-1,2-diphenylethylene diamine {(1*R*,2*R*)-DPEApy} and (1*S*,2*S*)-*N*,*N*′-bis-(isonicotinoyl)-1,2-cyclohexane diamine {(1*S*,2*S*)-CHDApy} chiral guests, are reported. Additions of (1*R*,2*R*)-DPEA and (1*S*,2*S*)-CHDA separately to **1** in dichloromethane result in the formation of 1:1 sandwich complexes **1**·DPEA$_{(R,R)}$ and **1**·CHDA$_{(S,S)}$, respectively, at low guest concentration and 1:2 anti complexes **1**·(DPEA$_{(R,R)}$)$_2$ and **1**·(CHDA$_{(S,S)}$)$_2$, respectively, at higher guest concentration. In contrast, separate additions of (1*R*,2*R*)-DPEApy and (1*S*,2*S*)-CHDApy to **1** produce only 1:1 sandwich complexes of **1**·DPEApy$_{(R,R)}$ and **1**·CHDApy$_{(S,S)}$, respectively. The binding constants at 295 K between **1** and (1*R*,2*R*)-DPEA are observed to be (4.7 ± 0.2) × 10^4 M^{-1} and (4.3 ± 0.3) × 10^3 M^{-1} for 1:1 sandwich and 1:2 anti form, respectively, while the respective values with (1*S*,2*S*)-CHDA are (1.5 ± 0.2) × 10^5 M^{-1} and (5.9 ± 0.3) × 10^3 M^{-1}. However, much larger values of (2.5 ± 0.3) × 10^5 M^{-1} and (1.3 ± 0.3) × 10^6 M^{-1} have been observed with DPEApy$_{(R,R)}$ and CHDApy$_{(S,S)}$, respectively, to produce the corresponding 1:1 sandwich complexes. **1**·DPEApy$_{(R,R)}$ (A_{cal}, −1759 cm^{-1} M^{-1}) (A_{cal} = $\Delta\varepsilon_1 - \Delta\varepsilon_2$, representing the total amplitude of the calculated circular dichroism (CD) couplets) shows ∼10-fold increase in CD amplitude compared to the values observed for **1**·DPEA$_{(R,R)}$ (A_{cal}, +187 cm^{-1} M^{-1}), while **1**·CHDApy$_{(S,S)}$ (A_{cal}, +1886 cm^{-1} M^{-1}) shows nearly 3-fold increase of the CD amplitude compared to the value observed for **1**·CHDA$_{(S,S)}$ (A_{cal}, −785 cm^{-1} M^{-1}) at 295 K. The A_{cal} values of −1759 cm^{-1} M^{-1} and +1886 cm^{-1} M^{-1} observed for the **1**·DPEApy$_{(R,R)}$ and **1**·CHDApy$_{(S,S)}$, respectively, are extremely high. To the best of our knowledge, these are some of the largest values reported for a chirality induction process involving bisporphyrin *tweezer* receptors. The large enhancement in the CD signal intensity is due to the well complementarity size between Zn(II)bisporphyrin host and the extended chiral diamines guest, which results large unidirectional twisting of two porphyrin units to accommodate the guests having preorganized binding sites with minimum host–guest steric interactions. It is interesting to note that **1**·DPEA$_{(R,R)}$ and **1**·DPEApy$_{(R,R)}$ show CD signal opposite in sign to each other, which happens to be the case between **1**·CHDA$_{(S,S)}$ and **1**·CHDApy$_{(S,S)}$ also.

INTRODUCTION

Determination of absolute configuration remains a very important topic in the chemical and biological world. Porphyrins are considered to be one of the most useful chromophores for probing molecular chirality because of their unique property of absorption spectroscopy, featuring intense Soret band at the visible region, which is an important

Received: June 2, 2013
Published: February 12, 2014

   dx.doi.org/10.1021/ic401395d | *Inorg. Chem.* 2014, 53, 2381−2395

prerequisite for efficient chirogenic performance.[1] Moreover, the facile methods of synthetic modification and metalation of the porphyrin core enhance the scope of choosing different types of chiral substrates. Formation of supramolecular complex between the metalloporphyrin as host and chiral substrate as guest through axial ligation enables induction of chirality information of the chiral guest to the achiral host.[1−10] As a result, a bisignate circular dichroism (CD) curve (so-called exciton couplet) is observed, with two bands of opposite sign and similar intensity centered around the λ_{max} of the UV−visible absorption, corresponding to the transition dipoles.[1] The sign of the CD couplet is determined by the interaction between electric transition moments associated with the chromophores' transitions. In the absorption spectrum, the magnitude of the shifts and splitting are correlated with the relative orientation and distance between the coupled electric transitions dipole moments associated with Soret band. The observed chiroptical response of the host−guest supramolecular complex is a direct consequence of the chirality of the substrate, which translates into the helicity of the interacting chromophores, and therefore the assignment of chirality is nonempirical.[1]

There are numerous supramolecular complexes between the metalloporphyrin *tweezer* as host and chiral[1−10]/achiral[11] substrate as guest through axial ligation. Achiral bisporphyrin *tweezer* receptors are powerful tools for the absolute configurational analysis of organic compounds using CD spectroscopy. Chirality is generated within the supramolecular complex due to the stereospecific twisting of the two bridged porphyrin units, caused by the enantiomerically pure chiral substrates to minimize the host−guest steric clash.[1,2] The complex exhibits an exciton couplet in the porphyrin Soret band region of the CD spectrum, whose sign is governed by the absolute configuration of the guest, while its amplitude depends on various external (i.e., temperature, pH, polarity of the medium, etc.) and internal factors (i.e., bond strength, stoichiometry, electronic effects, etc.). Substrates' preorganized coordinating sites, along with the differences in the effective size of the substituents around the chiral center, dictate the sign of the interporphyrin helical twist.[1,2] The experimentally observed CD and UV−visible spectra represent a weighted average of the corresponding spectra of the individual diastereoisomers present in the solution. The observation of low intensity in the CD signals have also been explained by partial cancellation of intense CD bands for the diastereoisomeric complexes that have opposite couplet sign.[2]

However, the underlying reason for the chirality transfer lies in the nature of the molecular recognition that takes place during the complexation process.[1] In the case of chiral assemblies consisting of two or more porphyrins, there are two major factors which make such studies very complicated: the dynamic nature of noncovalent assemblies and the complex electronic structure of the pigments as a consequence of the several possible orientations of the electronic transitions. A detailed understanding of the underpinning mechanisms and various influencing factors is of particular significance for smart control of the absolute stereochemical determination of a variety of chiral molecules. In the present Investigation, we report high enhancement of CD amplitude of the 1:1 sandwich complex comprising 1,1′-ferrocene carboxylate bridged Zn(II) bisporphyrin and the extended chiral substrates (1*R*,2*R*)-*N*,*N*′-bis-(isonicotinoyl)-1,2-diphenylethylene diamine {(1*R*,2*R*)-DPEApy} and (1*S*,2*S*)-*N*,*N*′-bis-(isonicotinoyl)-1,2-cyclohexane diamine {(1*S*,2*S*)-CHDApy} derived from their respective smaller chiral diamines, (1*R*,2*R*)-1,2-diphenylethylene diamine {(1*R*,2*R*)-DPEA} and (1*S*,2*S*)-1,2-cyclohexane diamine {(1*S*,2*S*)-CHDA}, whose 1:1 sandwich complexes, otherwise, gives relatively lower values. The two cyclopentadienyl (Cp) rings in ferrocene, which sandwich an iron(II) center, are parallel to each other and can also rotate freely even at low temperature.[12] In fact, $[(\eta^5\text{-}C_5H_4CO_2R)_2Fe]$ is already proven to be structurally very versatile because of the conformational freedom of the two cyclopentadienyl moieties around the coordination axis and, therefore, has been exploited as a module to bridge between two porphyrin rings in the present investigation.

RESULTS AND DISCUSSION

Ferrocene-bridged bisporphyrin (H_4FcTPP),[13] (1*R*,2*R*)-DPEApy,[14a] and (1*S*,2*S*)-CHDApy[14b] were synthesized following the procedures reported earlier. To the free base bisporphyrin H_4FcTPP in dichloromethane, an excess of zinc acetate was added and stirred at room temperature, yielding dark-red complex **1** in excellent yields upon chromatographic purification. The UV−visible spectrum of **1** in dichloromethane displays an intense Soret band at 420 nm and two Q bands at 548 and 585 nm.

The interaction of **1** with the chiral diamine substrates was first investigated by UV−visible spectroscopy. Addition of (1*R*,2*R*)-DPEA to **1** (1.0×10^{-6} M) in dichloromethane results in a small red-shifts of the Soret (from 420 to 422 nm) and Q bands (from 548 to 562 nm and 585 to 603 nm) along with appearance of a shoulder at 437 nm (Figure 1A) due to the formation of 1:1 host−guest complex **1**·DPEA$_{(R,R)}$, which was then isolated as solid in good yields and characterized. Observation of such a small red shift (of 2 nm) in the 1:1

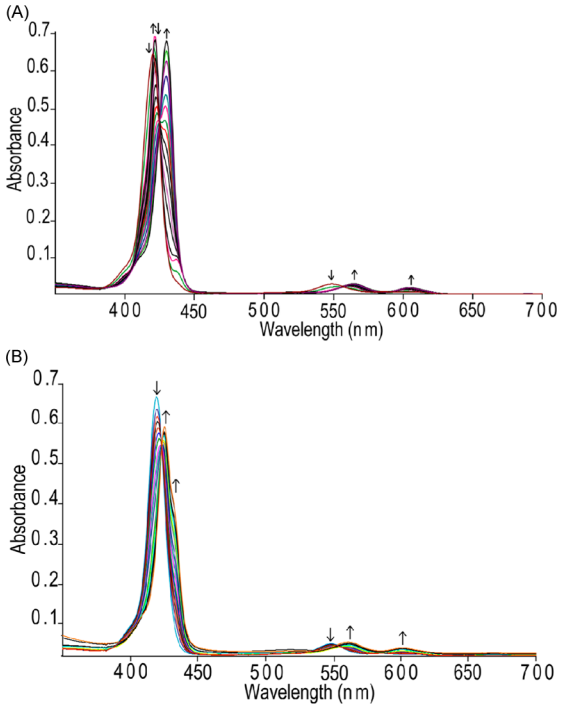

Figure 1. UV−visible spectral changes (at 295 K) of **1** (1.0×10^{-6} M) in dichloromethane upon addition of (A) (1*R*,2*R*)-DPEA as the host−guest molar ratio changes from 1:0 to 1:432 and (B) (1*R*,2*R*)-DPEApy as the host−guest molar ratio changes from 1:0 to 1:42.

dx.doi.org/10.1021/ic401395d | *Inorg. Chem.* 2014, 53, 2381−2395

Scheme 1

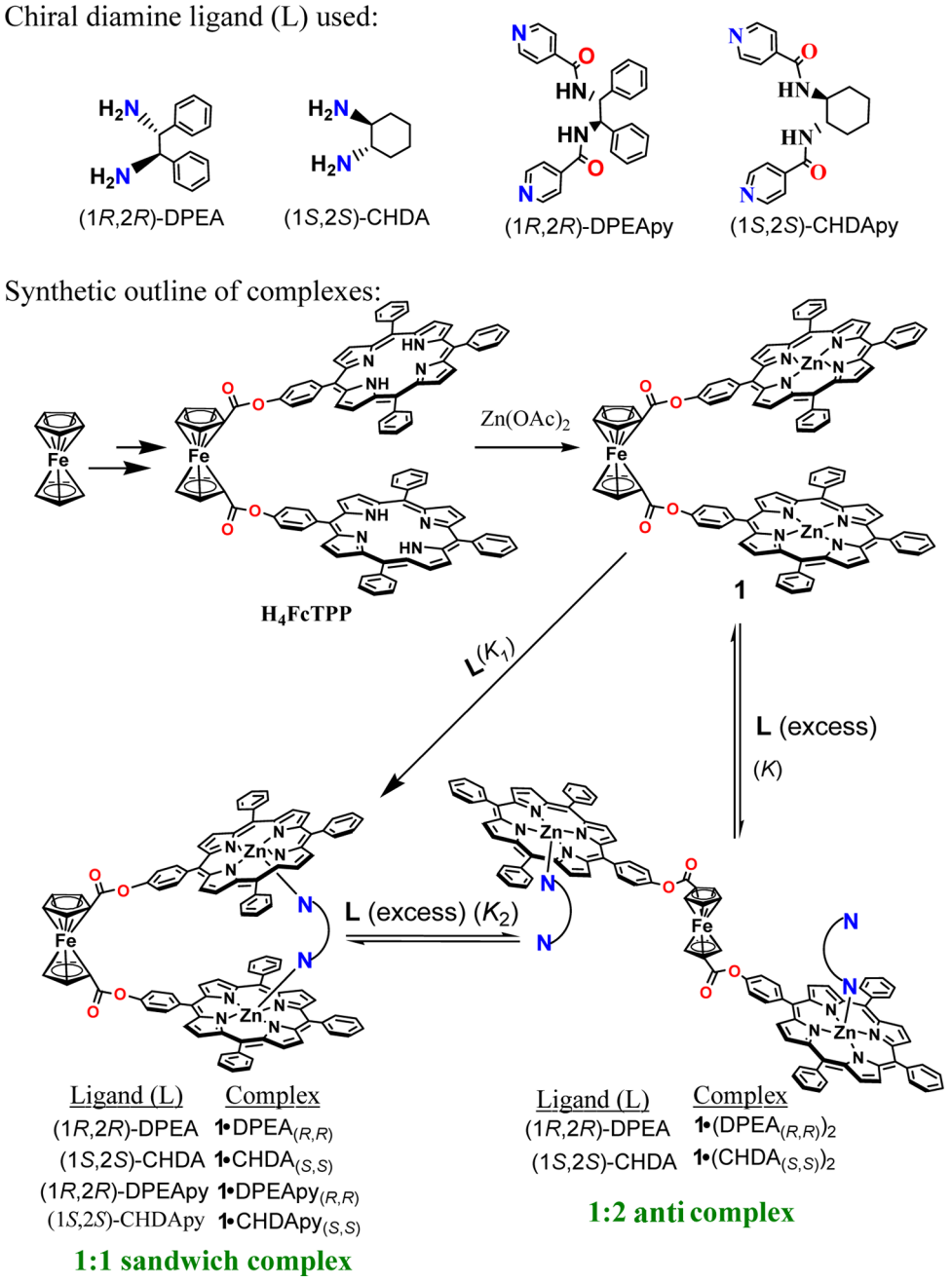

complex is due to the presence of strong interchromophore exciton coupling as the two porphyrin rings arranged in nearly cofacial manner and are separated by a small distance (vide infra). The Soret band at 422 nm and shoulder at 437 nm arise because of the low energy (in-phase) and high energy (out-of-phase) transitions, respectively. Addition of (1*S*,2*S*)-CHDA to **1** also brings out a similar UV−visible spectral change (Supporting Information, Figure S1) due to the formation of 1:1 host−guest complex **1**·CHDA$_{(S,S)}$, which was isolated as solid in good yield and characterized. However, the additions of a large excess of chiral diamine substrates result in large red shift (of 10 nm) of the Soret band up to 430 nm, which is characteristic[3b] of the formation of 1:2 anti complexes **1**·(DPEA$_{(R,R)}$)$_2$ and **1**·(CHDA$_{(S,S)}$)$_2$. Interestingly, the Soret band of the 1:2 anti complex, formed upon addition of excess monoamine such as 2-aminobutane into Zn(II)bisporphyrin, **1**, is also at 430 nm (Supporting Information, Figure S2).

Upon additions of extended chiral substrates (1*R*,2*R*)-DPEApy or (1*S*,2*S*)-CHDApy to **1**, a relatively large red shift of the Soret (from 420 to 425 nm) and Q bands (548 to 561 nm and 585 to 601 nm) along with a shoulder at 432 nm were observed, which are due to the formation of 1:1 host−guest complex **1**·DPEApy$_{(R,R)}$ and **1**·CHDApy$_{(S,S)}$ (Figure 1B and Supporting Information, Figure S3), respectively. The complexes were also isolated as solid in good yields and spectroscopically characterized. Unlike the case of smaller substrates DPEA and CHDA, there is no evidence of the formation of 1:2 host−guest complex even at very high concentration of extended chiral substrates DPEApy and CHDApy. Interestingly, the Soret band of the 1:2 anti complex,

dx.doi.org/10.1021/ic401395d | *Inorg. Chem.* 2014, 53, 2381−2395

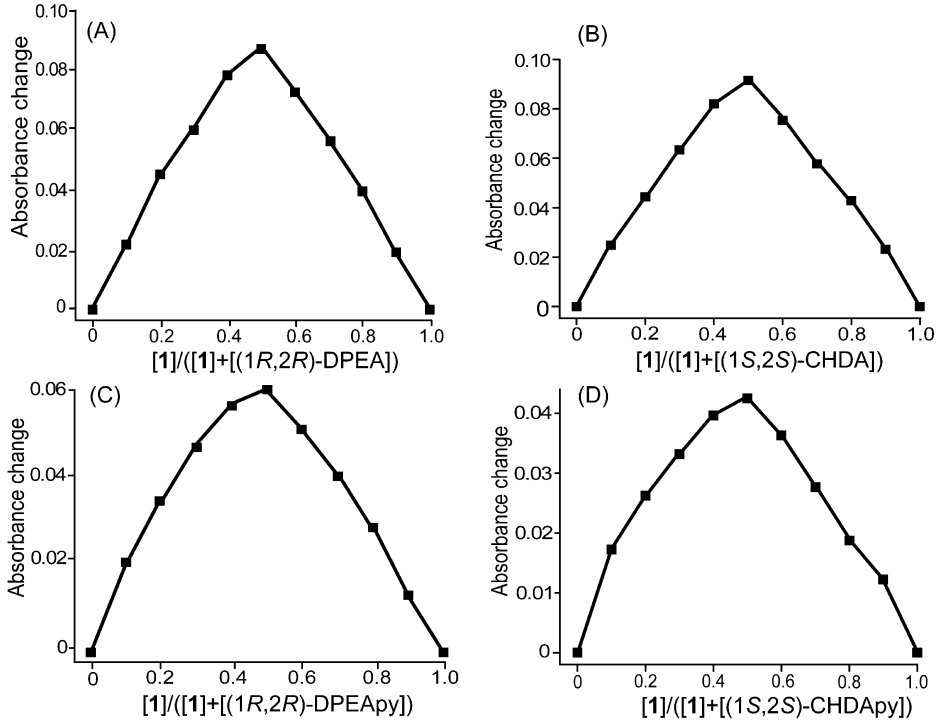

Figure 2. Job's plot establishing the 1:1 stoichiometry for the binding between **1** and (A) (1*R*,2*R*)-DPEA, (B) (1*S*,2*S*)-CHDA, (C) (1*R*,2*R*)-DPEApy, and (D) (1*S*,2*S*)-CHDApy in dichloromethane at 295 K.

formed upon addition of excess pyridine into **1**, appears at 427 nm (Supporting Information, Figure S4). Scheme 1 shows the synthetic outline of the complexes reported here, along with their abbreviations used in the present investigation, while detailed synthetic procedures and their spectral characterizations are given in the Experimental Section.

It is well-known that coordination of an amine group with the Zn(II)porphyrin results in a red shift of the Soret band.[6c] However, the extent of the red shift of the Soret band for the 1:1 sandwich complex depends on the separation of two interacting porphyrin planes; closely interacting porphyrin rings red shift to a lesser degree as opposed to porphyrin rings that are well-separated.[6c] This phenomenon can be explained as a result of two counteracting effects: binding of the amine to the Zn(II)bisporphyrin leads to large red shift, while blue shift of the absorption takes place as a result of bringing two porphyrin rings closer to each other in the 1:1 sandwich complex. In the present investigation, shift of the Soret band of **1** caused by extended diamine substrates is 5 nm while only 2 nm with the smaller substrates, which is obvious due to the greater interporphyrinic distance in the former because of the bigger size of the extended chiral substrates. The above spectral features are thus indicative of the formation of 1:1 sandwich complex at lower substrate concentration in the present investigation.

The host–guest 1:1 stoichiometry is determined by the Job's continuous variation plot (Figure 2). Absorbance change of **1** has been monitored at 422 nm (for the binding of (1*R*,2*R*)-DPEA and (1*S*,2*S*)-CHDA) and at 425 nm (for (1*R*,2*R*)-DPEApy and (1*S*,2*S*)-CHDApy), in which the optimum formation of 1:1 host–guest complex took place at their equimolar concentration (i.e., 0.5 mol fractions). Electrospray ionization (ESI) mass spectroscopy reveals peaks at *m*/*z* 2044.4509 and 1948.4506, which are assigned for $[\mathbf{1}\cdot DPEApy_{(R,R)}]^+$ (Supporting Information, Figure S5) and $[\mathbf{1}\cdot CHDApy_{(S,S)}+2H]^+$ (Supporting Information, Figure S6), respectively, confirming the formation of 1:1 complexes. The isotopic distribution patterns of the experimental mass were also nicely correlated with the theoretical patterns. Besides the ferrocene-bridged bisporphyrin (H_4FcTPP) receptor, we are unable to get the single crystals of the complexes suitable for X-ray structure determinations; however, **1** and $\mathbf{1}\cdot DPEApy_{(R,R)}$ have been geometrically optimized using density functional theory (DFT) (vide infra).

Crystallographic Characterization of H_4FcTPP. Dark-purple crystals of H_4FcTPP were grown via slow diffusion of *n*-hexane into a dichloromethane solution of the complex at room temperature in air. The molecule crystallizes in the monoclinic crystal system with *C*2/*c* space group; a perspective view is depicted in Figure 3, while crystal data and data collection

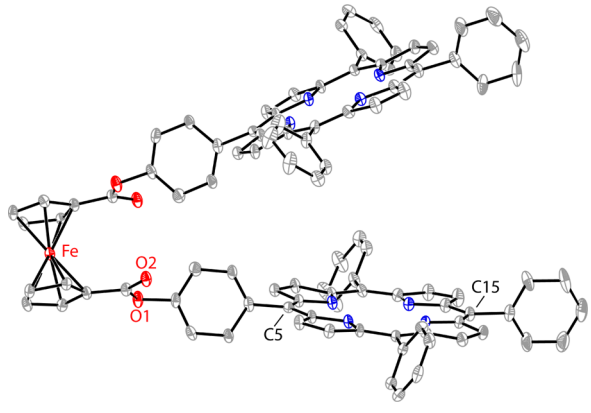

Figure 3. Perspective view of H_4FcTPP showing 50% thermal contours for all non-hydrogen atoms at 100 K (H atoms have been omitted for clarity).

dx.doi.org/10.1021/ic401395d | *Inorg. Chem.* 2014, 53, 2381–2395

parameters are listed in Table 1. A diagram illustrating the molecular packing in the crystal lattice is shown in Supporting Information, Figure S7. The porphyrin rings are planar with face-to-face arrangement, which makes a dihedral angle of 25.1° defined by two least-squares planes of $C_{20}N_4$ porphyrinato core. The mean plane separation between two porphyrin cores is found to be 9.09 Å, while the distance between two macrocyclic centers ($C_t \cdots C_t$) is 10.40 Å, which suggest no significant interactions between two rings. The torsion angle between the meso carbons C5, C15 and C5′, C15′ of the two porphyrin rings is 11.9°. Two Cp rings of the bridging 1,1′-ferrocene carboxylate are in gauche form with a twist angle of 17.6°. The twist angle between the two Cp rings can, however, vary from 0° to 180° with every possible angle due to the rotational freedom of the rings. For example, the twist angles between two Cp rings are observed to be 180°, 93.0°, and 1.6° in $[NH_2(CH_3)_2]_2[Fe(\eta^5\text{-}C_5H_4COO)_2]$,[12c] $[C_8H_{16}N_4]_2[Fe(\eta^5\text{-}C_5H_4COO)_2]\cdot 2C_2H_5OH$,[12d] and $Fe(\eta^5\text{-}C_5H_4COOH)_2$,[12e] respectively.

Table 1. Crystal Data and Data Collection Parameters

	H_4FcTPP
formula	$C_{100}H_{66}N_8O_4Fe_1$
T, K	100(2)
formula weight	1499.46
crystal system	monoclinic
space group	$C2/c$
a, Å	41.643(13)
b, Å	14.469(5)
c, Å	17.265(6)
α, deg	90.000
β, deg	113.899(7)
γ, deg	90.000
V, Å^3	9511(6)
radiation (λ, Å)	Mo Kα (0.71073)
Z	4
d_{calcd}, g cm^{-3}	1.047
$F(000)$	3119
μ, mm^{-1}	0.209
no. of unique data	8844
no. of parameters, refined	510
GOF on F^2	0.907
$R1^a$ [$I > 2\sigma(I)$]	0.089
$R1^a$ (all data)	0.1648
$wR2^b$ (all data)	0.2470
largest diff. peak and hole	0.873 and −0.330 e Å^{-3}

$^aR1 = \sum||F_o| - |F_c||/\sum|F_o|$. $^bwR2 = \{\sum[w(F_o^2 - F_c^2)^2]/\sum[w(F_o^2)^2]\}^{1/2}$.

^{1}H NMR. ^{1}H NMR plays an important role in suggesting 1:1 sandwich complexation in solution. Figure 4 shows the relevant spectra coming from the reaction between **1** and (1*R*,2*R*)-1,2 diphenylethylene diamine. Trace A shows the well-resolved ^{1}H NMR spectrum of **1** in $CDCl_3$, while trace B shows the spectra after the addition of 1.0 M equiv of (1*R*,2*R*)-DPEA due to the formation of **1**·DPEA$_{(R,R)}$. Identical spectrum was also obtained using the polycrystalline sample of the complex in $CDCl_3$. Trace C, however, shows the ^{1}H NMR spectrum of the free (1*R*,2*R*)-DPEA alone in $CDCl_3$. As can be seen, the ^{1}H NMR spectra of **1**·DPEA$_{(R,R)}$ (trace B) shows a large change from that of **1** and free (1*R*,2*R*)-DPEA substrate. The spectral pattern of the 1:1 host–guest complex observed here is very similar to that of the 1:1 sandwich complexes reported in the literature.[1,2] The notably large upfield shifts of the substrate's C*H* ($\Delta\delta$, 4.97 ppm) and NH_2 ($\Delta\delta$, 4.39 ppm) protons is supportive of substrate's capture within the bisporphyrin concave in the 1:1 host–guest complex.[1,2] In the porphyrin part also, there appear large changes. The two singlet peaks at 4.82 and 5.34 ppm shown by the bridging ferrocene protons of the Zn(II)-bisporphyrin **1** (trace A) are broadened and appear at 4.80 and 5.38 ppm (trace B), respectively, because of their exposure to a different ring current environment in the sandwich complex, which results from the stereospecific twisting of the two porphyrin units. Well-resolved four doublets assigned for pyrrole protons of the porphyrin ring in **1** are now transformed into four multiplets in the 1:1 sandwich complex.

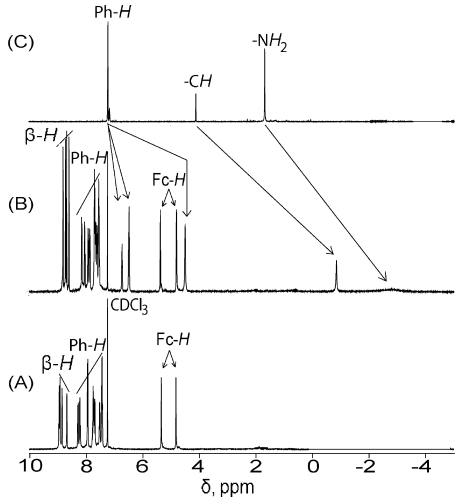

Figure 4. ^{1}H NMR spectra in $CDCl_3$ (at 295 K) of (A) **1**, (B) **1**·DPEA$_{(R,R)}$ and (C) (1*R*,2*R*)-DPEA.

Similar upfield shift of the guest's protons clamped between two porphyrin subunits have also been observed when **1** was titrated with (1*S*,2*S*)-CHDA. However, the extent of shifting in the ^{1}H NMR spectrum was much less when monomeric ZnTPP (TPP = tetraphenyl porphyrin) was titrated with the same substrate (vide infra). Figure 5 displays the ^{1}H NMR spectra of **1**, substrate, and 1:1 host–guest complex. There are remarkable upfield shifts of the substrate's protons H^5 ($\Delta\delta$, 5.69 ppm) and NH_2 ($\Delta\delta$, 6.61 ppm), as they are embedded within the ring current effect of the bisporphyrin cavity, which is supportive of substrate's capture within the bisporphyrin concave to form a 1:1 sandwich complex.[1,2] Two singlet peaks at 4.82 and 5.34 ppm shown by the bridging ferrocene protons of the Zn(II)bisporphyrin **1** (trace A) are now split into four singlets at 4.78, 4.76 and 5.40, 5.38 ppm (trace B), respectively, because of their exposure to a different ring current environment. Furthermore, four well-resolved doublets signifying the pyrrole protons of porphyrin ring in **1** have been transformed into two doublets and one multiplet in the 1:1 sandwich complex.

It is appropriate to compare now the ^{1}H NMR spectra between **1**·DPEA$_{(R,R)}$ and **1**·CHDA$_{(S,S)}$. The spectral patterns look very similar; guest protons are all upfield-shifted, while NH_2 protons are shifted most, followed by other protons. However, the upfield shift of the NH_2 protons is much more in **1**·CHDA$_{(S,S)}$, which suggests much stronger binding of CHDA substrate to **1** compared to DPEA, as also observed experimentally (vide infra).

dx.doi.org/10.1021/ic401395d | Inorg. Chem. 2014, 53, 2381–2395

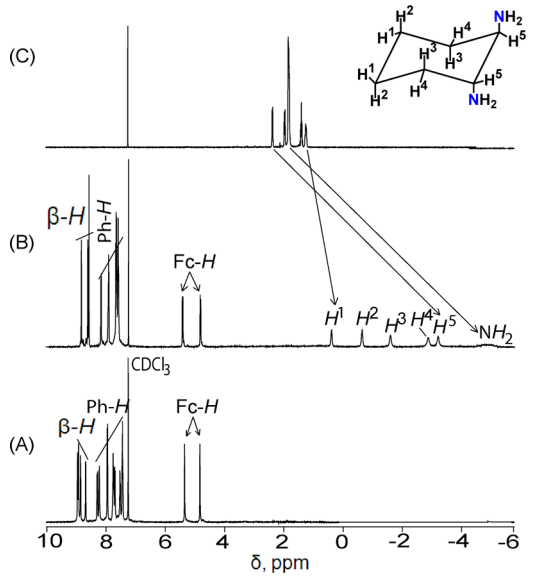

Figure 5. ^{1}H NMR spectra in $CDCl_3$ (at 295 K) of (A) **1**, (B) **1**·$CHDA_{(S,S)}$, and (C) (1*S*,2*S*)-CHDA. Inset shows the proton numbering scheme of CHDA substrate.

As observed in the case of **1**·$DPEA_{(R,R)}$ and **1**·$CHDA_{(S,S)}$, all the protons of the extended chiral substrates are also found to be upfield-shifted in the ^{1}H NMR, which supports the encapsulation of the substrates inside the bisporphyrin cavity, resulting in intramolecular 1:1 sandwich complexes **1**·$DPEApy_{(R,R)}$ and **1**·$CHDApy_{(S,S)}$ in solution. The porphyrin ring current affects the pyridine protons of the extended chiral substrates most since they are in close proximity to the porphyrin ring. For **1**·$DPEApy_{(R,R)}$, the pyridine protons, which are closer to the porphyrin ring, are the most upfield-shifted ($\Delta\delta$, 6.09 ppm), while phenyl protons of the substrate are less upfield-shifted ($\Delta\delta$, 0.73 ppm), as displayed in Figure 6. Similarly, there are several changes in the porphyrin part also. The two singlet peaks, shown by the bridging ferrocene protons of the Zn(II)bisporphyrin, have been split into four singlets at 4.77, 4.82 and 5.31, 5.33 ppm in the 1:1 sandwich complex

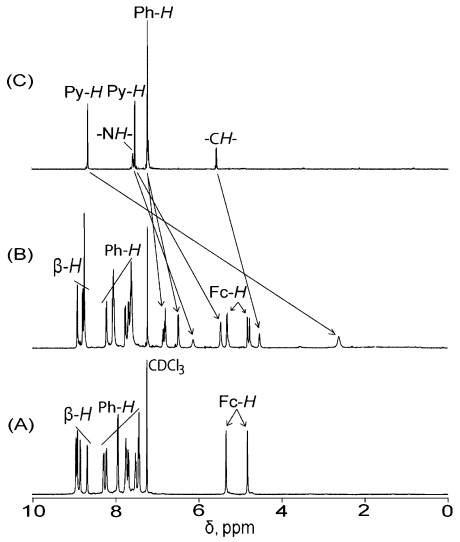

Figure 6. ^{1}H NMR spectra in $CDCl_3$ (at 295 K) of (A) **1**, (B) **1**·$DPEApy_{(R,R)}$, and (C) (1*R*,2*R*)-DPEApy.

(trace B). Moreover, four well-resolved doublets observed for the pyrrole protons of porphyrin rings in **1** are transformed into two doublets and one multiplet in the sandwich complex. For **1**·$CHDApy_{(S,S)}$, similar spectral changes in the ^{1}H NMR are also observed, as demonstrated in Figure 7. Two pyridine

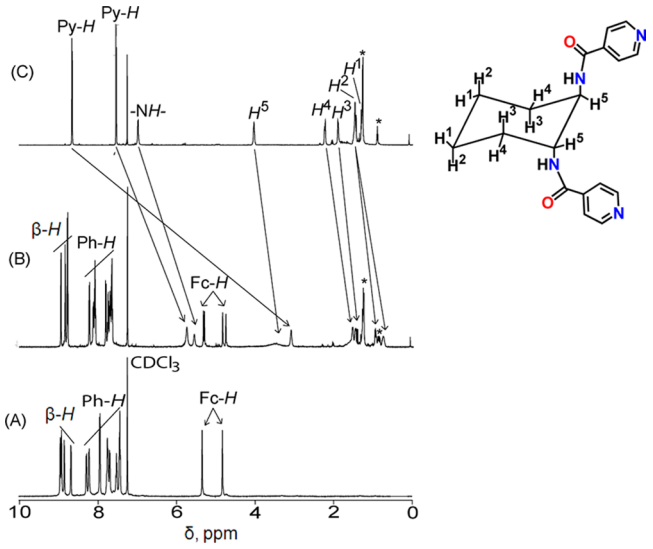

Figure 7. ^{1}H NMR spectra in $CDCl_3$ (at 298 K) of (A) **1**, (B) **1**·$CHDApy_{(S,S)}$, and (C) (1*S*,2*S*)-CHDApy (asterisk represents solvent or trace impurity). Inset shows the proton numbering scheme of CHDApy substrate.

proton signals of the substrate are upfield-shifted by 5.58 and 1.8 ppm. Bridging ferrocene protons have also been split into four singlets at 4.75, 4.83, 5.30, and 5.32 ppm in the 1:1 sandwich complex. Porphyrin ring pyrrolic protons are also changed to two doublets and one multiplet in the complex.

Complete assignment of the resonances for all the complexes have been made on the basis of relative intensities of the signals and a ^{1}H−^{1}H COSY experiment, as demonstrated in Figures 8

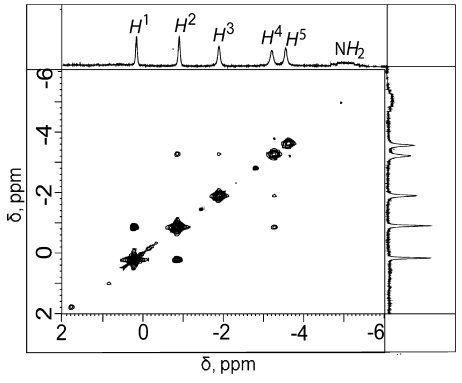

Figure 8. ^{1}H−^{1}H COSY spectrum of **1**·$CHDA_{(S,S)}$ in $CDCl_3$ at 295 K (selected portion only).

and S8−S11 (see Supporting Information). The spectral patterns of 1:1 host−guest complexes observed in the present Investigation are similar to the 1:1 sandwich complexes reported earlier.[1,2]

^{13}C NMR. ^{13}C NMR spectra were recorded at 295 K in $CDCl_3$, which also plays important role in supporting the formation of the 1:1 sandwich complexes in solution. The spectra are displayed in Figures 9, 10, and S12−S18 (see

dx.doi.org/10.1021/ic401395d | Inorg. Chem. 2014, 53, 2381−2395

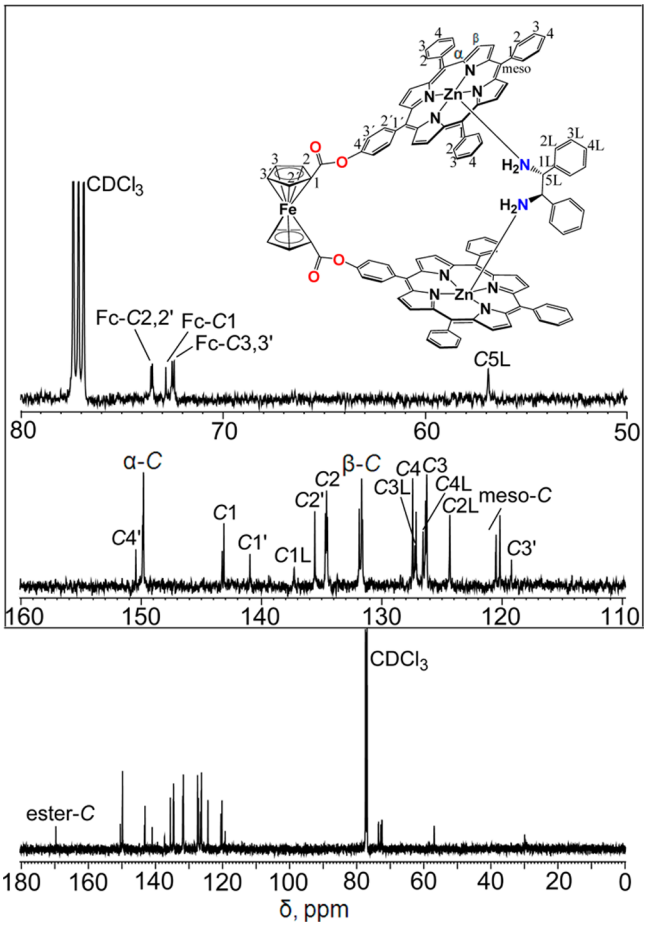

Figure 9. ^{13}C NMR spectrum of **1**·DPEA$_{(R,R)}$ in $CDCl_3$ at 295 K. Inset shows the expanded regions of the spectrum, along with atom numbering scheme used to assign the ^{13}C peaks.

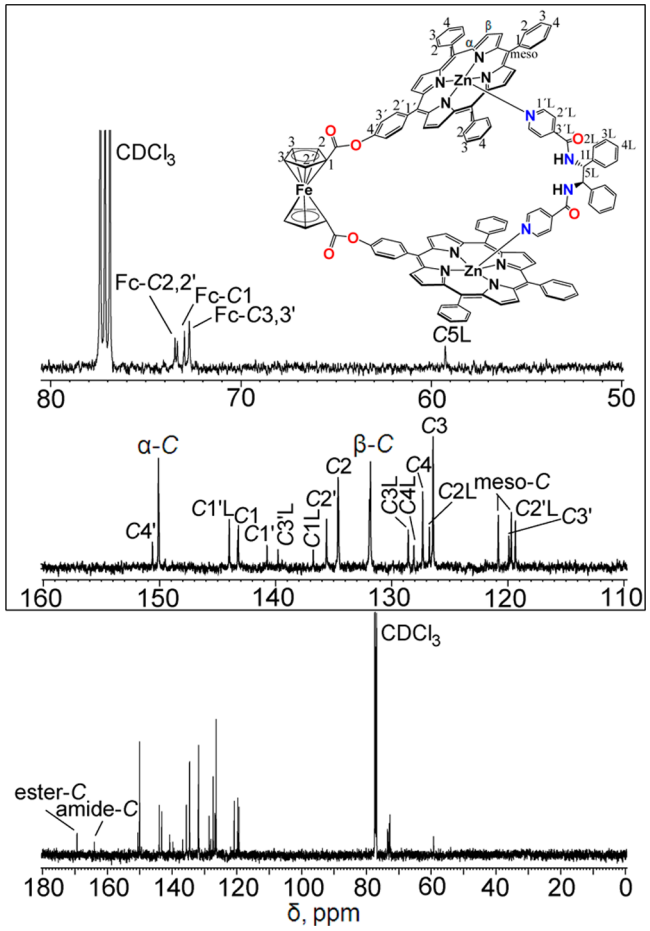

Figure 10. ^{13}C NMR spectrum of **1**·DPEApy$_{(R,R)}$ in $CDCl_3$ at 295 K. Inset shows the expanded regions of the spectrum, along with atom numbering scheme used to assign the ^{13}C peaks.

Supporting Information) for all the complexes and substrates reported here. As seen in the ^{1}H NMR spectra, large upfield shift of the ^{13}C resonances were also observed for the chiral diamine substrates sandwiched between two porphyrin rings in the 1:1 complexes reported here. For example, large upfield shifts are observed for C1L ($\Delta\delta$, 6.03 ppm) and C5L ($\Delta\delta$, 5.05 ppm) that are related to DPEA in **1**·DPEA$_{(R,R)}$ (Figure 9) and for C1L ($\Delta\delta$, 6.53 ppm), C2L ($\Delta\delta$, 5.73 ppm), and C3L ($\Delta\delta$, 3.09 ppm) that are related to CHDA in **1**·CHDA$_{(S,S)}$ (Supporting Information, Figure S17). In case of **1**·DPEApy$_{(R,R)}$ (Figure 10) also, pyridine carbons of the extended chiral substrate C1′L, C2′L, and C3′L are upfield-shifted by 6.05, 1.99, and 1.71 ppm, respectively, while the same carbons are upfield-shifted by 6.69, 1.57, and 0.98, respectively, in **1**·CHDApy$_{(S,S)}$ (Supporting Information, Figure S18). Large changes were also observed in the porphyrin part of the 1:1 sandwich complexes. It is interesting to note that the bridging ferrocene carbons Fc-C2 and Fc-C3 are no longer identical with Fc-C2′ and Fc-C3′, respectively, because of the stereospecific twisting of the two porphyrin rings in the sandwich complexes. As a result, each of the ^{13}C resonances in **1** that arise from carbons of Fc-C2, Fc-C2′, Fc-C3, and Fc-C3′ are split into two resonances in the 1:1 sandwich complexes reported here.

Binding Constant Determination. Binding constants between **1** and the chiral diamines are determined by UV–visible spectroscopic titration method. The addition of (1*S*,2*S*)-CHDA (10^{-7} to 10^{-4} M) to the dichloromethane solution of **1** (1×10^{-6} M) at 295 K initially results in the red shift of Soret (420 to 422 nm) and Q bands (548 to 562 nm, 585 to 603 nm), due to the formation of 1:1 sandwich complex. Addition of a large excess of CHDA ligand causes further red shift of Soret band to 430 nm and Q bands to 565 and 605 nm, respectively, due to the formation of 1:2 anti complex. The binding constants were calculated using the HypSpec computer program (Protonic Software, U.K.), and species distribution plots of the complex were calculated using the program HySS2009 (Protonic Software, U.K.).[15] Three sets of UV–visible titration data were analyzed, considering a binding model with three colored stoichiometric states of Zn(II)-bisporphyrin (**1**), 1:1 host–guest complex, and 1:2 anti complex, as shown in Scheme 1. For complexation between **1** and (1*S*,2*S*)-CHDA, K_1 and K_2 are found to be $(1.5 \pm 0.2) \times 10^5$ M^{-1} and $(5.9 \pm 0.3) \times 10^3$ M^{-1}, respectively (Figure 11).

Similarly, the binding constants between **1** and (1*R*,2*R*)-DPEA are also determined by the UV–visible spectroscopic titration method. The addition of (1*R*,2*R*)-DPEA (10^{-7} to 10^{-4} M) to a dichloromethane solution of **1** (1×10^{-6} M) at 295 K also results in a similar spectral change. K_1 and K_2 (Supporting Information, Figure S19) are found to be $(4.7 \pm 0.2) \times 10^4$ M^{-1} and $(4.3 \pm 0.3) \times 10^3$ M^{-1}, respectively.

Gradual additions of (1*S*,2*S*)-CHDApy (10^{-7} to 10^{-5} M) to a dichloromethane solution of **1** (1×10^{-6} M) at 295 K results in a large red shift of the Soret band from 420 to 425 nm, due to the formation of 1:1 sandwich complex. We also analyzed two

dx.doi.org/10.1021/ic401395d | Inorg. Chem. 2014, 53, 2381–2395

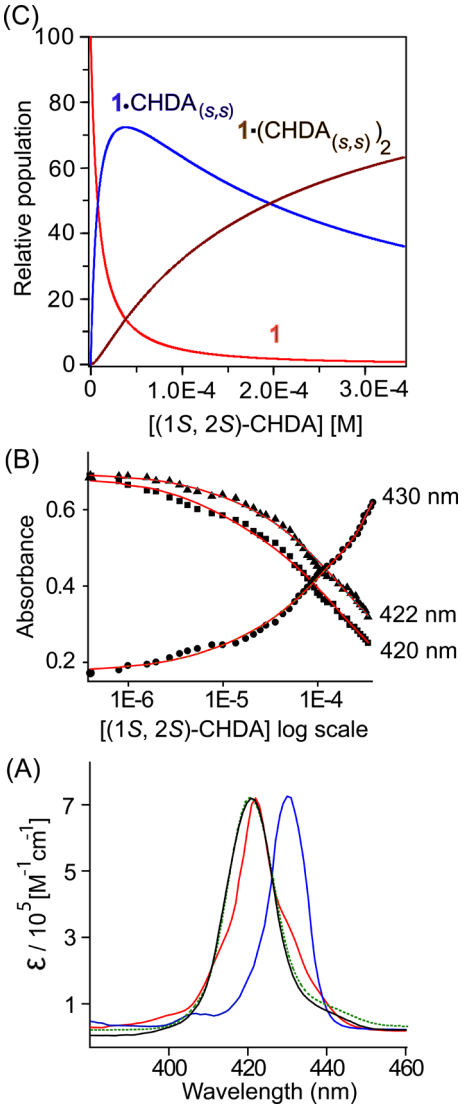

Figure 11. (A) Calculated UV−visible spectra of (black) **1**, (red) **1**·CHDA$_{(S,S)}$, and (blue) **1**·(CHDA$_{(S,S)}$)$_2$. Green dotted line represents the observed UV−visible spectra of **1**. (B) Fits of the absorbance data at selected wavelengths of 420, 422, and 430 nm. (C) Species distribution plots of **1**, **1**·CHDA$_{(S,S)}$, and **1**·(CHDA$_{(S,S)}$)$_2$ complexes.

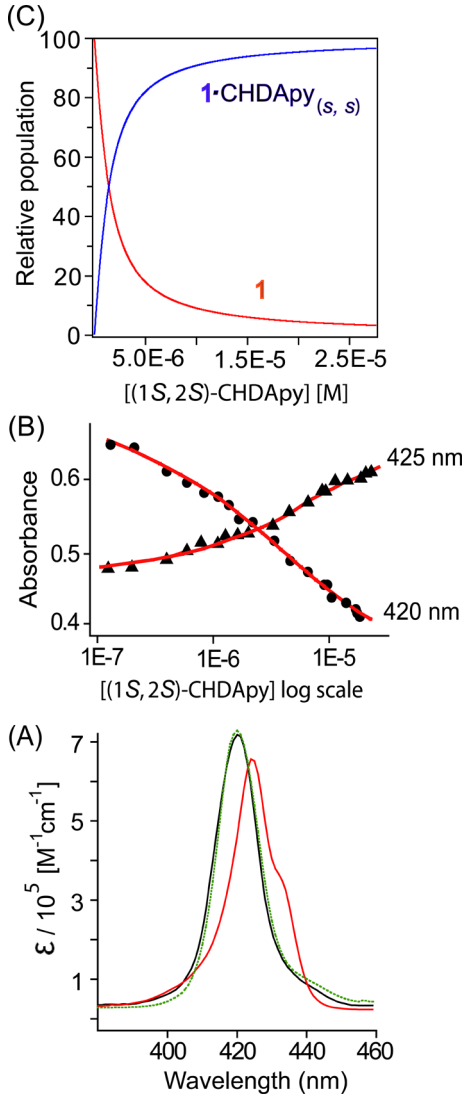

Figure 12. (A) Calculated UV−visible spectra of (black) **1** and (red) **1**·CHDApy$_{(S,S)}$. Green dotted line represents the observed UV−visible spectra of **1**. (B) Fits of the titration data at selected wavelengths of 420 and 425 nm. (C) Species distribution plots of **1** and **1**·CHDApy$_{(S,S)}$ complex.

sets of UV−visible titration data using the HypSpec program package considering a binding model with the two colored stoichiometric states of Zn(II)bisporphyrin (**1**) and 1:1 sandwich complex (Figure 12). The binding constant K that is obtained from the binding model is $(1.3 \pm 0.3) \times 10^6$ M^{-1}. Similar spectral changes were also observed when the other extended chiral substrate (1*R*,2*R*)-DPEApy (10^{-7} to 10^{-5} M) was added to **1** (1×10^{-6} M); K is found to be $(2.5 \pm 0.3) \times 10^5$ M^{-1} (Supporting Information, Figure S20).

As can be seen from the relative population plots shown above, both the 1:1 sandwich and the 1:2 anti form of the complexes are present in the solution at a given concentration when smaller chiral diamine substrates are used to titrate with the Zn(II)bisporphyrin **1**. However, the populations of the 1:1 complex are greater at lower substrate concentrations, while the addition of a large excess of chiral diamine results in the increase of the 1:2 anti form. In contrast, the addition of the extended chiral substrate forms 1:1 sandwich complex exclusively. The calculated UV−visible spectra of the complexes are also displayed in Figures 11, 12, S19, and S20 (see Supporting Information). As can be seen, calculated UV−visible spectra of the receptor **1** are nearly identical with the observed one.

From the binding constant values, it can be concluded that extended chiral diamine binds much more strongly with **1** than with their respective smaller ligands due to the well-matched sizes between host and guest molecules (vide infra) that results in favorable geometry of the former. **1** is flexible enough to bind smaller diamines as well in spite of the mismatch of host−guest sizes but at the cost of greater strain that leads to the weaker binding constants. The binding constant value of $(2.5 \pm 0.3) \times 10^5$ M^{-1}, observed for DPEApy ligand for the 1:1 sandwich complex, is nearly 5 times larger compared to the value of $(4.7 \pm 0.2) \times 10^4$ M^{-1} observed for the similar complex with smaller DPEA ligand. For the same reasons, CHDApy binds ∼8 times more strongly than does CHDA ($(1.5 \pm 0.2) \times 10^5$ M^{-1}) with **1**. Furthermore, the binding constant of DPEA with **1** is smaller than that of CHDA, which is due to the presence of bulky

dx.doi.org/10.1021/ic401395d | Inorg. Chem. 2014, 53, 2381−2395

phenyl groups in DPEA that generates significant steric clash with the bisporphyrin moiety.

CIRCULAR DICHROISM

Circular dichroism (CD) has become a versatile tool for studying the supramolecular chirality induction phenomena.[1] Upon coordination of the nonracemic chiral substrate to the metal center of the bisporphyrin, there appears a CD signal at the Soret band region of the bisporphyrin. The sign of the CD signal is the reflection of the interchromophore twist; a clockwise twist generates a positive CD signal, while anticlockwise twist produces negative CD signal.[1,2]

We also have monitored the host–guest interaction by CD spectroscopy in the present investigation. Addition of (1*R*,2*R*)-DPEA to the dichloromethane solution of **1** (1×10^{-6} M) leads to the increase of positive bisignate CD response at the Soret band region, showing an optimum value at about 20 equiv of substrate, which then started to decrease upon further addition (Figure 13) due to stepwise equilibrium shift toward the 1:2

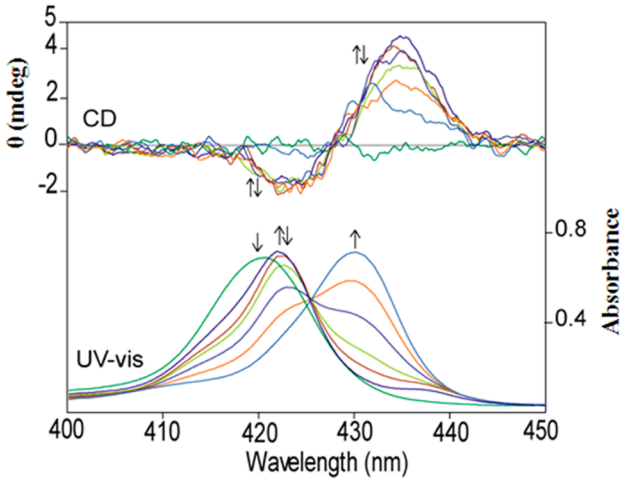

Figure 13. Selected spectra of (top) CD and (bottom) UV–visible titrations of **1** (1×10^{-6} M) in CH_2Cl_2 with (1*R*,2*R*)-DPEA as the host–guest molar ratio changes from 1:0 to 1:340 at 295 K.

anti complex. CD spectroscopy thus confirms the formation of 1:1 sandwich complex **1**·DPEA$_{(R,R)}$. Upon addition of large excess of the (1*R*,2*R*)-DPEA, CD amplitude declines toward zero, indicating conversion of the 1:1 sandwich to 1:2 anti complex.[3,4] On the other hand, addition of (1*R*,2*R*)-DPEApy to **1** at 295 K produces only the 1:1 sandwich complex with very high CD amplitude of -1759 cm^{-1} M^{-1}, which does not change upon further addition of guest substrate because of the strong host–guest binding in the complex (Figure 14). The UV–visible and CD spectra of **1**, **1**·DPEA$_{(R,R)}$, and **1**·DPEApy$_{(R,R)}$ are compared in Figure 15. As can be seen, the CD amplitude is almost 10-fold larger in **1**·DPEApy$_{(R,R)}$ as compared to the value observed in **1**·DPEA$_{(R,R)}$. Such an enhanced negative CD couplet observed in **1**·DPEApy$_{(R,R)}$ is supported by the large negative torsion angle (Φ) of $-21.95°$ obtained from the DFT optimized structure of the complex (vide infra). However, the sign of CD signal shown by **1**·DPEA$_{(R,R)}$ is opposite to that of **1**·DPEApy$_{(R,R)}$.

Similarly, the interaction of (1*S*,2*S*)-CHDA with Zn(II)-bisporphyrin **1** (1×10^{-6} M) was also monitored using CD spectroscopy, which showed optimum CD amplitude at about 10 equiv of CHDA substrate and then started to decrease upon

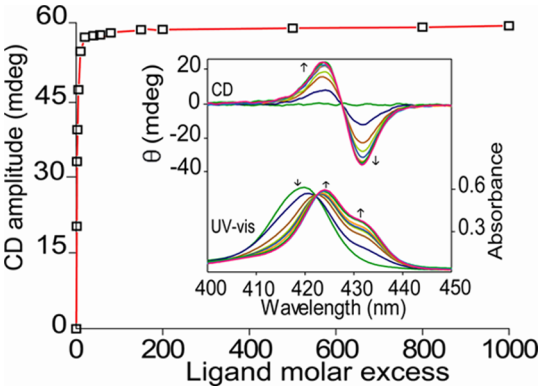

Figure 14. Change of CD amplitude upon addition of (1*R*,2*R*)-DPEApy to the CH_2Cl_2 solution of **1** (1×10^{-6} M) at 295 K as the host–guest molar ratio changes from 1:0 to 1:1000. Inset shows the respective changes in CD and UV–visible spectra upon addition of guest substrate.

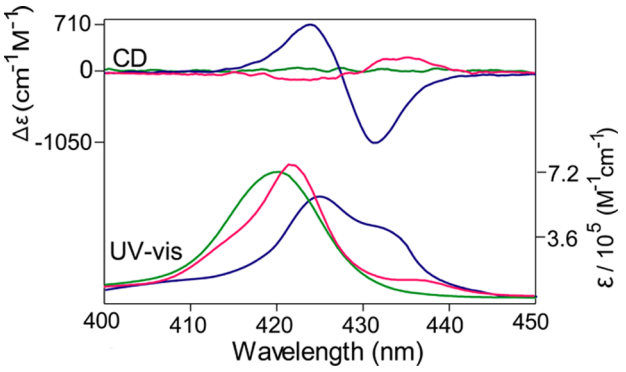

Figure 15. CD and UV–visible spectra of (green) **1**, (red) **1**·DPEA$_{(R,R)}$, and (blue) **1**·DPEApy$_{(R,R)}$ in dichloromethane solution of **1** (1×10^{-6} M) at 295 K.

further addition of the substrate, as shown in Figure 16. At the substrate's excess molar ratio, CD amplitude declines toward zero, indicating conversion of the 1:1 sandwich complex **1**·CHDA$_{(S,S)}$ to the 1:2 anti complex **1**·(CHDA$_{(S,S)}$)$_2$.[3,4] On the

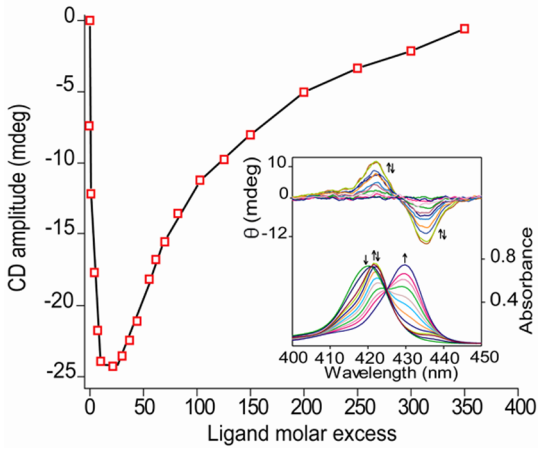

Figure 16. Change of CD amplitude upon addition of (1*S*,2*S*)-CHDA to the CH_2Cl_2 solution of **1** (1×10^{-6} M) at 295 K as the host–guest molar ratio changes from 1:0 to 1:360. Inset shows the respective changes in CD and UV–visible spectra upon addition of guest substrate.

dx.doi.org/10.1021/ic401395d | *Inorg. Chem.* 2014, 53, 2381–2395

other hand, addition of (1*S*,2*S*)-CHDApy to **1** (1×10^{-6} M) at 295 K produces only the 1:1 sandwich complex **1**·CHDApy$_{(S,S)}$ with very high CD amplitude of +1886 cm^{-1} M^{-1}, which does not change upon further addition of substrate, as shown in Figure 17. The UV–visible and CD spectra of both the

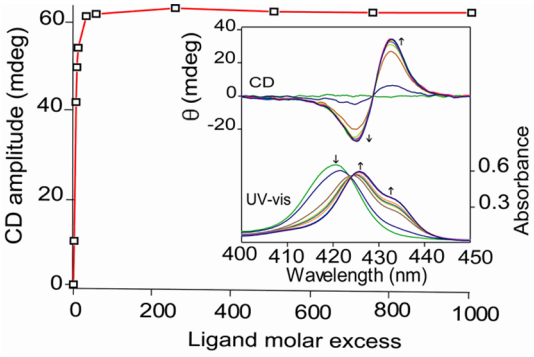

Figure 17. CD amplitude change upon addition of (1*S*,2*S*)-CHDApy to the CH_2Cl_2 solution of **1** (1×10^{-6} M) at 295 K as the host–guest molar ratio changes from 1:0 to 1:1000. Inset shows the respective changes in CD and UV–visible spectra upon addition of guest substrate.

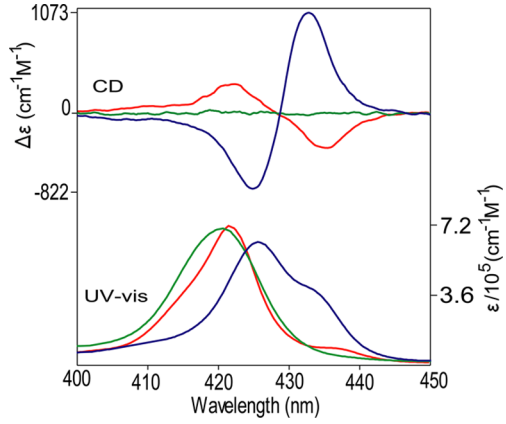

Figure 18. CD and UV–visible spectra of (green) **1**, (red) **1**·CHDA$_{(S,S)}$, and (blue) **1**·CHDApy$_{(S,S)}$ in dichloromethane solution of **1** (1×10^{-6} M) at 295 K.

complexes are compared in Figure 18. As can be seen, the CD amplitude is nearly 3-fold higher in **1**·CHDApy$_{(S,S)}$ as compared to the value obtained in **1**·CHDA$_{(S,S)}$. Such a large enhancement of the CD amplitude in **1**·CHDApy$_{(S,S)}$, as compared to **1**·CHDA$_{(S,S)}$, is due to the higher stability and favorable geometry of the former complex. (1*S*,2*S*)-CHDApy is accommodated by **1** more comfortably than is (1*S*,2*S*)-CHDA, whose interni-trogen distances between two binding sites are 9.067 Å and 2.925 Å, respectively.[2,14b] As discussed earlier for **1**·DPEApy$_{(R,R)}$, such an intense positive CD signal for **1**·CHDApy$_{(S,S)}$ is due to large unidirectional clockwise twisting of the two porphyrin units dictated by the preorganized binding sites of (1*S*,2*S*)-CHDApy.

We also fitted the CD titration data between **1** and chiral substrates using the HypSpec computer program (Protonic Software, U.K.),[15] which enables us to calculate the binding constants and also generate the corresponding CD spectra for the 1:1 sandwich complexes. Figures 19, S21, and S22 (see

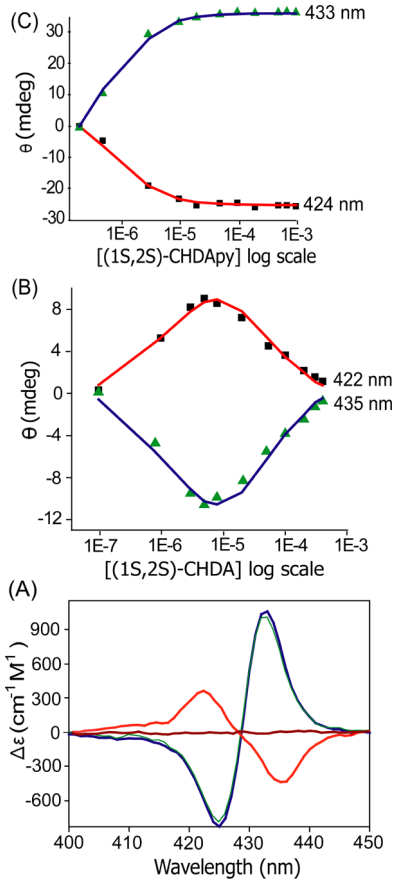

Figure 19. (A) Calculated CD spectra of (red) **1**·CHDA$_{(S,S)}$, (gray) **1**·(CHDA$_{(S,S)}$)$_2$, (blue) **1**·CHDApy$_{(S,S)}$, and (green) observed CD spectra of **1**·CHDApy$_{(S,S)}$. (B) Fits of the titration data of **1** with (1*S*,2*S*)-CHDA to the theoretical binding isotherm at selected wavelengths of 422 and 435 nm. (C) Fits of the titration data of **1** with (1*S*,2*S*)-CHDApy to the theoretical binding isotherm at selected wavelengths of 424 and 433 nm.

Supporting Information) compares the calculated and experimental CD spectra along with binding isotherms at selected wavelengths for the complexes reported here. The binding constants obtained separately from UV–visible and CD titration data also correlates nicely, as shown in Table 2, which also summarizes the CD spectral parameters for all the complexes.

As can be seen from Figures 19, S21, and S22 (see Supporting Information), very good agreements are obtained between calculated and observed CD spectra of the 1:1 sandwich complex when extended chiral substrates (1*S*,2*S*)-CHDApy and (1*R*,2*R*)-DPEApy are used. This is because of the exclusive formation of 1:1 sandwich complexes **1**·DPEApy$_{(R,R)}$ and **1**·CHDApy$_{(S,S)}$ in solution. However, the calculated bisignate CD amplitude of 1:1 sandwich complexes are greater than the observed one when smaller chiral diamines {(1*S*,2*S*)-CHDA and (1*R*,2*R*)-DPEA} are used to titrate with Zn(II)bisporphyrin **1**. In these cases, the population of 1:1 sandwich species can never be exclusive in solution since some proportion of 1:2 anti complexes will always be there, as shown earlier (vide infra).

However, the sign of the CD couplet shown by the 1:1 sandwich complex involving extended chiral substrate (1*R*,2*R*)-DPEApy is opposite to that of the sandwich complex involving (1*R*,2*R*)-DPEA even though both the substrates have the same

dx.doi.org/10.1021/ic401395d | Inorg. Chem. 2014, 53, 2381–2395

Table 2. Calculated CD Spectral Data and Binding Constants of the Complexes at 295 K

	1:1-sandwich complex CD data, λ (nm) [$\Delta\varepsilon$ (M^{-1} cm^{-1})]				1:2-anti complex CD data, λ (nm) [$\Delta\varepsilon$ (M^{-1} cm^{-1})]		
compound	FC[a]	SC[a]	A_{cal}[b]	binding constant K_1 $(M^{-1})^{c,d}$	FC[a]	SC[a]	binding constant K_2 $(M^{-1})^{c,d}$
1·DPEA$_{(R,R)}$	435[+127]	424[−60]	+187	$(4.7 \pm 0.2) \times 10^4$ $[(5.2 \pm 0.3) \times 10^4]$	negligible	negligible	$(4.3 \pm 0.3) \times 10^3$ $[(4.5 \pm 0.3) \times 10^3]$
1·CHDA$_{(S,S)}$	435[−424]	423[+361]	−785	$(1.5 \pm 0.2) \times 10^5$ $[(2.0 \pm 0.3) \times 10^5]$	negligible	negligible	$(5.9 \pm 0.3) \times 10^3$ $[(6.1 \pm 0.3) \times 10^3]$
1·DPEApy$_{(R,R)}$	432[−1031]	424[+728]	−1759	$(2.5 \pm 0.3) \times 10^5$ $[(2.6 \pm 0.3) \times 10^5]$			
1·CHDApy$_{(S,S)}$	432[+1076]	424[−810]	+1886	$(1.3 \pm 0.3) \times 10^6$ $[(1.3 \pm 0.3) \times 10^6]$			

[a]FC: first Cotton effect; SC: second Cotton effect. [b]A_{cal} (= $\Delta\varepsilon_1 - \Delta\varepsilon_2$) represents the total amplitude of the calculated CD couplets. [c]Calculated from UV−visible spectral measurement. [d]Values shown within the [brackets] are calculated from CD spectral measurement.

stereocenters. Since the phenyl groups of the chiral substrate are situated far away from the porphyrin rings in **1**·DPEApy$_{(R,R)}$, no significant steric clash can be possible between the substituents at the chiral center and porphyrin. Therefore, preorganized projection of the two pyridyl coordinating sites of (1*R*,2*R*)-DPEApy is the only cause of disposition of two porphyrin subunits, which results in anticlockwise twisting of the two porphyrin rings. Moreover, a nonbonding Zn···Zn distance of 12.307 Å was obtained in **1**, which is very much suitable for binding the extended chiral substrate (1*R*,2*R*)-DPEApy, whose internitrogen distance between two binding sites was found to be 9.390 Å (vide infra). The higher stability and favorable geometry of **1**·DPEApy$_{(R,R)}$ results in larger unidirectional twisting (left-handed) of the two porphyrin units to accommodate the guest having preorganized binding sites with minimum steric interactions, which eventually leads to such a large enhancement in the CD amplitude.

As proposed by Borhan et al.,[6e] during the 1:1 sandwich formation with the chiral substrates, the largest group on the chiral center should be in anti with respect to the bound chromophores to ensure minimum steric interactions. Two possible arrangements are demonstrated in Figure 20 for the binding of (1*R*,2*R*)-DPEA with **1**; the largest groups (Ph on C1 and C2) can be placed either in anti or in syn position to the coordinating amines. This steric differentiation would lead to the counterclockwise rotation of the porphyrin P-1 and a clockwise rotation of porphyrin P-2, which would eventually result in a positive helical arrangement of the 1:1 sandwich complex (and hence positive CD signal), as observed in **1**·DPEA$_{(R,R)}$. Induction of positive CD signal (A_{cal} = +364 cm^{-1} M^{-1}) in the 1:1 sandwich complex has also been reported with (1*R*,2*R*)-DPEA using pentanedioxy bridged bis-Zn(II) [5-(4-carboxyphenyl)-10,15,20-tri(pentafluorophenyl) porphyrin] as a receptor.[6e]

In our earlier report,[2] we also have observed the positive sign of the CD couplet for the 1:1 sandwich complex formed between diphenyl ether-bridged Zn(II)bisporphyrin host and (1*R*,2*R*)-DPEA guest. The X-ray structure of the complex contains two molecules in the asymmetric unit in which the porphyrin rings are twisted in clockwise and anticlockwise directions around the bridging group, with tortional angles of +34.5(7)° and −33.1(7)° for molecules I and II, respectively. The low CD amplitude of the 1:1 sandwich complex was due to the presence of both right- and left-handed screws of the molecule.[2] Similar situation is also expected for **1**·DPEA$_{(R,R)}$ reported here, where both the clockwise and anticlockwise twisting of the two porphyrin rings are possible. The resultant

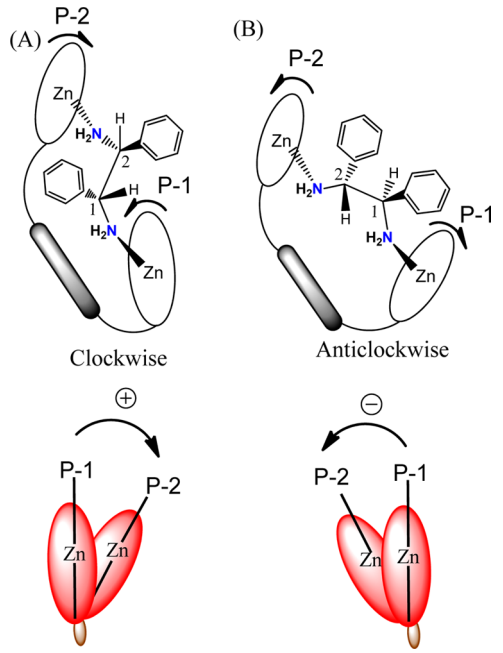

Figure 20. Proposed binding schemes between **1** and (1*R*,2*R*)-DPEA, resulting (A) clockwise and (B) anticlockwise conformers.

weak positive CD signal expressed by the 1:1 sandwich complex comes from the contribution of the clockwise twisted sandwich complex surpassing the contribution of anticlockwise twisted one.

As observed between **1**·DPEA$_{(R,R)}$ and **1**·DPEApy$_{(R,R)}$, the sign of the CD couplet shown by the 1:1 sandwich complex involving extended chiral substrate (1*S*,2*S*)-CHDApy is also opposite to that shown by the complex involving smaller (1*S*,2*S*)-CHDA, even if the two substrates have identical chirality. Contrary to the general observation[1−10] of positive CD couplet expected with (1*S*,2*S*)-CHDA, surprisingly negative CD couplet is observed here by **1**·CHDA$_{(S,S)}$. According to the chirality exciton theory, negative CD couplet is related to the anticlockwise twist of the two porphyrin units. Computational study of the 1:1 sandwich complex consistsing of similar TPP-type Zn(II)bisporphyrin and the same chiral (1*S*,2*S*)-CHDA substrate was performed recently, which, however, predicts a small difference in energy (relative energy 0.6 kcal/mol) between two diastereoisomers, with a clockwise and an anticlockwise orientation of two porphyrin rings.[3a] Ballester et al. have also reported a 1:1 sandwich complex of 4-

dx.doi.org/10.1021/ic401395d | *Inorg. Chem.* 2014, 53, 2381−2395

benzyloxypyridine-2,6-dicarboxyl bridged bis-Rh(III)I_2[5-(3-aminophenyl)-10,15,20-(tri-(4-pentyl)-phenyl)porphyrin] with (1*R*,2*R*)-CHDA, which shows positive CD couplet, in contrast to the "expected" negative CD couplet.[3a]

It is appropriate to discuss the binding of chiral diamine substrates with the monomeric ZnTPP host here. Addition of (1*S*,2*S*)-CHDA to ZnTPP (1×10^{-6} M) in dichloromethane also results in large red shifts of Soret (418 to 426 nm) and Q bands (from 547 to 561 nm and 585 to 602 nm). Supporting Information, Figure S23 displays the relevant ^{1}H NMR spectra from the reaction of ZnTPP with (1*S*,2*S*)-CHDA, which shows large upfield shift of CHDA protons of the host–guest complex. For example, upfield shifts of 4.40 and 4.85 ppm were observed for H^5 and NH_2 protons, respectively. However, the extent of shifts is much less than what was observed for the corresponding dimeric complex **1**·CHDA$_{(S,S)}$ (Figure 5) reported here. Interaction of ZnTPP with (1*S*,2*S*)-CHDA was also monitored by CD spectroscopy which, however, results in negligible response, in contrast to very large bisignate CD signal observed for **1**·CHDA$_{(S,S)}$ (Supporting Information, Figure S24).

COMPUTATIONAL STUDY

In the absence of X-ray structures, geometry optimization of **1** (Figure 21A) and **1**·DPEApy$_{(R,R)}$ (Figure 21B) have been performed with the help of DFT using the Gaussian 03,[16] revision B.04, package. It is important to note that **1**, whose nonbonding Zn···Zn distance is 12.307 Å, as evident from the optimized molecular structure, can more comfortably accommodate the extended chiral substrate (1*R*,2*R*)-DPEApy than (1*R*,2*R*)-DPEA, whose internitrogen distances between two binding sites are 9.390 Å and 2.896 Å, respectively.[2] This represents a highly favorable situation for (1*R*,2*R*)-DPEApy that results in a very large binding constant value. Anticlockwise twisting of the two porphyrin macrocycles in **1**·DPEApy$_{(R,R)}$ can be seen in the DFT-optimized structure of the complex in which the torsion angle Φ (C15–C5–C5′-C15′) is −21.95°. From this large interporphyrin anticlockwise twist, it is anticipated that the complex will show highly amplified negative CD signal, which is also observed experimentally. On examination of the Corey–Pauling–Koltun (CPK) molecular model shown in Figure 22, it can be seen that the two porphyrin units are twisted in an anticlockwise direction with minimum host–guest steric interactions. In contrast, the presence of two bulky phenyl substituents in (1*R*,2*R*)-DPEA, along with a much smaller interdiamine distance, generates large steric repulsion and geometrical constraint in the 1:1 sandwich complex, leading to much weaker binding of the substrate, which therefore converts to the 1:2 anti complex at the substrates high concentration region.

CONCLUSIONS

1,1′-ferrocene dicarboxylate bridged Zn(II)bis(*meso*-tetraphenyl)porphyrin **1** has been utilized to serve as a host molecule to hold chiral diamine substrates. **1** is highly flexible and hence is well-suited to accommodate small substrates (1*R*,2*R*)-DPEA and (1*S*,2*S*)-CHDA as well as their corresponding extended substrates (1*R*,2*R*)-DPEApy and (1*S*,2*S*)-CHDApy. Stepwise additions of smaller chiral substrates (1*R*,2*R*)-DPEA and (1*S*,2*S*)-CHDA initially form 1:1 sandwich complexes **1**·DPEA$_{(R,R)}$ and **1**·CHDA$_{(S,S)}$, respectively, while addition of a large excess of the substrate causes the 1:1

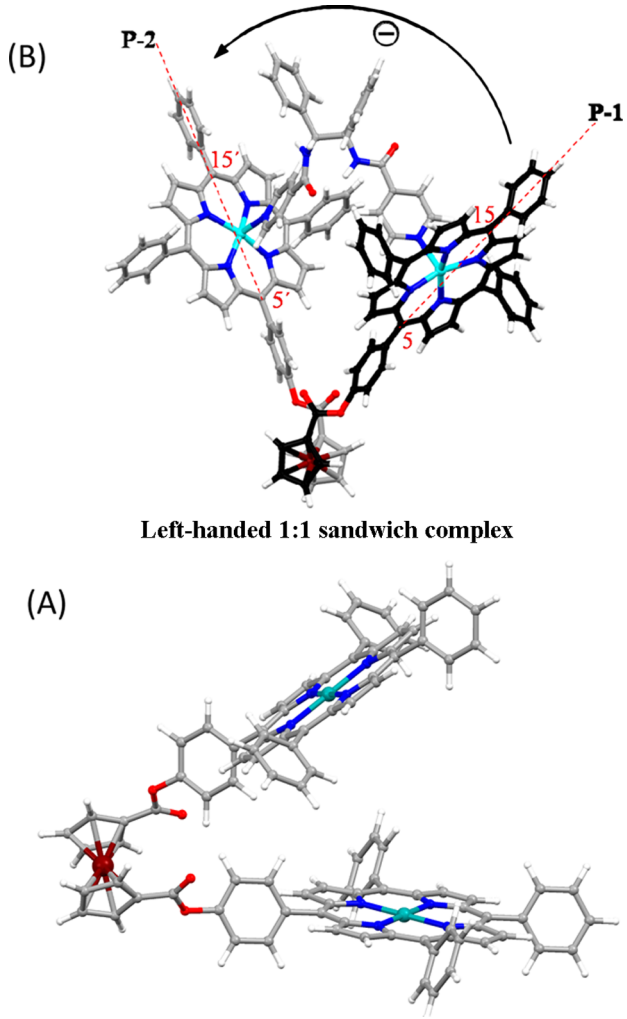

Figure 21. Optimized molecular structures of (A) **1** by DFT method at the B3LYP/6-31G** level and (B) **1**·DPEApy$_{(R,R)}$ by DFT method at the B3LYP/LANL2DZ level.

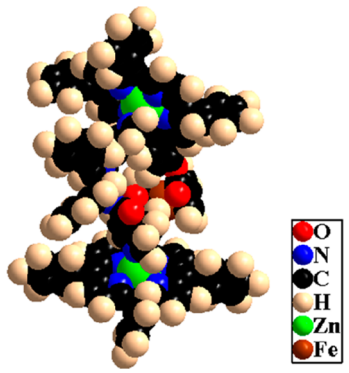

Figure 22. CPK molecular model of left-handed 1:1 sandwich complex **1**·DPEApy$_{(R,R)}$.

sandwich complexes to switch over to the corresponding anti complexes **1**·(DPEA$_{(R,R)}$)$_2$ and **1**·(CHDA$_{(S,S)}$)$_2$, respectively. However, extended chiral substrates (1*R*,2*R*)-DPEApy and (1*S*,2*S*)-CHDApy produce 1:1 sandwich complexes **1**·DPEApy$_{(R,R)}$ and **1**·CHDApy$_{(S,S)}$ exclusively. Zn(II) bisporphyrin **1**, whose nonbonding Zn···Zn distance is found to be 12.307 Å, can more comfortably accommodate the extended chiral substrate (1*R*,2*R*)-DPEApy than (1*R*,2*R*)-DPEA, whose inter-

dx.doi.org/10.1021/ic401395d | *Inorg. Chem.* 2014, 53, 2381–2395

nitrogen distances between two binding sites are 9.390 Å and 2.896 Å, respectively. Similarly, (1*S*,2*S*)-CHDApy is accommodated by **1** more easily than (1*S*,2*S*)-CHDA, whose internitrogen distances between two binding sites are 9.067 Å and 2.925 Å, respectively. This represents a highly favorable geometry for (1*R*,2*R*)-DPEApy and (1*S*,2*S*)-CHDApy with **1** that results in very large binding constants.

^{1}H and ^{13}C NMR of the complexes have played a very important role in unveiling the formation of 1:1 sandwich complex in solution. ^{1}H NMR reveals that all the substrate protons have remarkably large upfield shifts as the guest ligand immerges within the porphyrin ring current environment in sandwich complex. For the similar reason, all the resonances of the substrate carbons are also shifted to the upfield region in ^{13}C NMR.

The total amplitude of the CD couplet (A_{cal}) of −1759 cm^{-1} M^{-1} and +1886 cm^{-1} M^{-1} observed for the **1**·DPEApy$_{(R,R)}$ and **1**·CHDApy$_{(S,S)}$ complexes, respectively, at 295 K are extremely high. To the best of our knowledge, these are some of the largest values reported so far for a chirality-induction process involving bisporphyrin *tweezer* receptors. The A_{cal} value is nearly 10-fold higher in **1**·DPEApy$_{(R,R)}$ than the value observed for **1**·DPEA$_{(R,R)}$ while nearly 3-fold higher in **1**·CHDApy$_{(S,S)}$ compared to **1**·CHDA$_{(S,S)}$. The higher stability and favorable geometry of the 1:1 sandwich complex involving extended chiral guests result in larger unidirectional twisting of the two porphyrin units to accommodate the guests having preorganized binding sites with minimum steric interactions, which eventually leads to such a large enhancement in the CD amplitude. The steric differentiation for the binding of (1*R*,2*R*)-DPEA with **1** leads to a positive helical arrangement of the 1:1 sandwich complex (and hence positive CD signal), as observed in **1**·DPEA$_{(R,R)}$. The observed low CD intensity in case of **1**·DPEA$_{(R,R)}$ may also be accounted for by the conformational freedom of the complex to twist in both the clockwise and anticlockwise direction due to weaker and unfavorable binding of DPEA. It is interesting to note that 1:1 sandwich complexes of **1**·DPEA$_{(R,R)}$ and **1**·DPEApy$_{(R,R)}$ show CD signal opposite in sign to each other, which happens to be the case between **1**·CHDA$_{(S,S)}$ and **1**·CHDApy$_{(S,S)}$ also.

The present Investigation offers a great degree of insight into the structural factors responsible for chiral recognition and the amplitude of exciton couplets. The consideration and judicious application of these controlling factors can allow the rational production of smart molecular and chiroptical devices.

EXPERIMENTAL SECTION

Materials. The synthesis of the ferrocene-bridged bisporphyrin (H_4FcTPP) is accomplished by following the literature method.[13] Extended chiral substrates (1*R*,2*R*)-DPEApy and (1*S*,2*S*)-CHDApy were synthesized according to the procedure reported earlier.[14] Reagents and solvents are purchased from commercial sources and purified by standard procedures before use.

(1R,2R)-DPEApy. Anal. Calcd (Found): C, 73.92 (73.98); H, 5.25 (5.20); N, 13.26 (13.22)%. ^{1}H NMR ($CDCl_3$, 295 K): 8.69 (*d*, 4H, Py-*H*); 7.59 (*br*, 2H, −N*H*); 7.56 (*d*, 4H, Py-*H*); 7.24 (*m*, 10H, Ph-*H*); 5.60 (*dd*, 2H, −C*H*) ppm.

(1S,2S)-CHDApy. Anal. Calcd (Found): C, 66.65 (66.69); H, 6.21 (6.18); N, 17.27 (17.22)%. ^{1}H NMR ($CDCl_3$, 295 K): 8.67 (*d*, 4H, Py-*H*); 7.54 (*d*, 4H, Py-*H*); 6.97 (*br*, 2H, −N*H*); 4.02 (*m*, 2H, H^5); 2.21 (*m*, 2H, H^4); 1.87 (*m*, 2H, H^3); 1.43 (*m*, 2H, H^2); 1.27 (*m*, 2H, H^1) ppm.

H_4FcTPP. Anal. Calcd (Found): C, 80.10 (80.16); H, 4.44 (4.39); N, 7.47 (7.42)%. ^{1}H NMR ($CDCl_3$, 295 K): 9.04−8.74 (*m*, 16H, *β*-*H*); 8.44−8.34 (*m*, 8H, Ph(por)-*H*); 8.01 (*m*, 8H, Ph(por)-*H*); 7.83 (*m*, 10H, Ph(por)-*H*); 7.63 (*m*, 4H, Ph(por)-*H*); 7.50 (*m*, 8H, Ph(por)-*H*); 5.37 (*br*, 4H, Fc-*H*); 4.78 (*br*, 4H, Fc-*H*); −2.57(*s*, 2H, N*H*); −2.63(*s*, 2H, N*H*) ppm. ^{1}H NMR is shown in Supporting Information, Figure S25.

Zn-bisporphyrin, 1. 50 mg (0.033 mmol) of H_4FcTPP was taken in 20 mL of dichloromethane. An excess of $Zn(OAc)_2{\cdot}2H_2O$ was added to it, and it was stirred at room temperature for 1 h. Dichloromethane (50 mL) was added to the reaction mixture, which was washed with water three times. The solvent was dried over anhydrous Na_2SO_4, filtered, and evaporated to dryness. The solid residue was then purified by column chromatography on silica gel using dichloromethane as eluant. Yield: 49 mg (90%). M. P.: > 300 °C, ESI-MS: *m*/*z* 1624.2958 ([M + 2H]$^+$), Anal. Calcd (Found): C, 73.86 (73.92); H, 3.84 (3.79) N, 6.89 (6.84)%. UV−visible (CH_2Cl_2) [λ_{max}, nm (ε, M^{-1} cm^{-1})]: 420 (7.13 × 10^5), 548 (2.94 × 10^4), 585 (5.64 × 10^3). ^{1}H NMR ($CDCl_3$, 295 K): 8.97 (*d*, 4H, *β*-*H*); 8.94 (*d*, 4H, *β*-*H*); 8.86 (*d*, 4H, *β*-*H*); 8.69 (*d*, 4H, *β*-*H*); 8.31(*d*, 4H, Ph(por)-*H*); 8.23(*d*, 4H, Ph(por)-*H*); 7.95 (*d*, 8H, Ph(por)-*H*); 7.76 (*m*, 6H, Ph(por)-*H*); 7.69 (*d*, 4H, Ph(por)-*H*); 7.53 (*m*, 4H, Ph(por)-*H*); 7.44 (*t*, 8H, Ph(por)-*H*); 5.34 (*s*, 4H, Fc-*H*); 4.82 (*s*, 4H, Fc-*H*). ^{13}C NMR ($CDCl_3$, 295 K): 169.35 (2C, ester-*C*); 150.27 (2C, *C*4′); 150.22 (16C, *α*-*C*); 142.66 (6C, *C*1); 139.40 (2C, *C*1′); 135.35 (4C, *C*2′); 134.53−134.31 (12C, *C*2); 132.04 (16C, *β*-*C*); 127.60−127.34 (6C, *C*4); 126.66−126.39 (12C, *C*3); 121.16−120.06 (8C, *meso*-*C*); 119.32(4C, *C*3′); 73.79 (4C, Fc-*C*2,2′); 73.08 (2C, Fc-C1); 72.66(4C, Fc-C3,3′) ppm.

The 1:1 sandwich complexes reported in the present Work were prepared using the general procedure; details for one representative case are described below.

Synthesis of 1·DPEA$_{(R,R)}$. Zn-bisporphyrin **1** (50 mg, 0.031 mmol) was dissolved in 5 mL of distilled dichloromethane. Enantiomerically pure (1*R*,2*R*)-diphenylethylenediamine (7.9 mg, 0.037 mmol) was added to the solution, which was stirred for 30 min. The solution obtained was then filtered off to remove any solid residue and carefully layered with hexane in air at room temperature. On standing for 6 to 7 d, dark green crystalline solid precipitated out, which was then isolated by filtration, washed well with *n*-hexanes, and dried well in vacuum. Yield: 44 mg (78%). M. P.: > 300 °C, Anal. Calcd (Found): C, 74.47 (74.38); H, 4.28 (4.37) N, 7.62 (7.73)%. UV−visible (CH_2Cl_2) [λ_{max}, nm]: 422, 562, 603. ^{1}H NMR ($CDCl_3$, 295 K): 8.82 (*m*, 4H, *β*-*H*); 8.74 (*m*, 4H, *β*-*H*); 8.70 (*m*, 4H, *β*-*H*); 8.62 (*m*, 4H, *β*-*H*); 8.17−7.25 (*m*, 38H, Ph(por)-*H*); 6.73 (*m*, 2H, Ph-*H*, DPEA); 6.48 (*m*, 4H, Ph-*H*, DPEA); 5.38 (*m*, 4H, Fc-*H*); 4.80 (*m*, 4H, Fc-*H*); 4.50 (*m*, 4H, Ph-*H*, DPEA); −0.86 (*s*, 2H, −C*H*, DPEA); −2.75 (*br*, 4H, −NH_2, DPEA) ppm. ^{13}C NMR ($CDCl_3$, 295 K): 169.68 (2C, ester-*C*); 150.45 (2C, *C*4′); 149.89−149.82 (16C, *α*-*C*); 143.27−143.13 (6C, *C*1); 140.97 (2C, *C*1′); 137.40 (2C, *C*1L); 135.57 (4C, *C*2′); 134.69−134.52 (12C, *C*2); 131.88−131.62 (16C, *β*-*C*); 127.44, 127.15 (6C, *C*4); 127.26 (4C, *C*3L); 126.58 (2C, *C*4L); 126.37−126.27 (12C, *C*3); 123.82 (4C, *C*2L); 120.50−120.18 (8C, *meso*-*C*); 119.23 (4C, *C*3′); 73.56 (2C, Fc-*C*2); 73.49 (2C, Fc-*C*2′); 72.83 (2C, Fc-*C*1); 72.52 (2C, Fc-*C*3); 72.41 (2C, Fc-*C*3′); 56.92 (2C, *C*5L) ppm.

Synthesis of 1·CHDA$_{(S,S)}$. Yield: 44 mg (82%), M. P.: > 300 °C, Anal. Calcd (Found): C, 73.15 (73.09); H, 4.40 (4.55) N, 8.05 (8.11)%. UV−visible (CH_2Cl_2) [λ_{max}, nm]: 422, 562, 603. ^{1}H NMR ($CDCl_3$, 295K): 8.88 (*d*, 4H, *β*-*H*); 8.66 (*d*, 4H, *β*-*H*); 8.62 (*m*, 8H, *β*-*H*); 8.21 (*d*, 4H, Ph(por)-*H*); 7.94 (*m*, 8H, Ph(por)-*H*); 7.69−7.59 (*m*, 26H, Ph(por)-*H*); 5.40 (*s*, 2H, Fc-*H*); 5.38 (*s*, 2H, Fc-*H*); 4.78 (*s*, 2H, Fc-*H*); 4.76 (*s*, 2H, Fc-*H*); 0.25 (*m*, 2H, CHDA); −0.79 (*m*, 2H, CHDA); −1.76 (*m*, 2H, CHDA); −3.07 (*m*, 2H, CHDA); −3.41 (*m*, 2H, CHDA); −4.90 (*br*, 4H, NH_2, CHDA) ppm. ^{13}C NMR ($CDCl_3$, 295K): 169.41 (2C, ester-*C*); 150.49 (2C, *C*4′); 149.76−149.64 (16C, *α*-*C*); 143.28, 143.16 (6C, *C*1); 140.77 (2C, *C*1′); 135.70 (4C, *C*2′); 134.69−134.45 (12C, *C*2); 131.73−131.65 (16C, *β*-*C*); 127.22 (6C, *C*4); 126.46 (12C, *C*3); 120.59, 120.36, 120.03 (8C, *meso*-*C*); 119.56 (4C, *C*3′); 73.54 (2C, Fc-*C*2); 73.38 (2C, Fc-*C*2′); 72.86 (2C, Fc-*C*1); 72.60 (2C, Fc-*C*3); 72.37 (2C, Fc-*C*3′); 51.29 (2C, *C*1L); 29.93 (2C, *C*2L); 22.46 (2C, *C*3L) ppm.

Synthesis of 1·DPEApy$_{(R,R)}$. Yield: 53 mg (84%). M. P.: > 300 °C, ESI-MS: *m*/*z* 2044.4509 ([M]$^+$). Anal. Calcd (Found): C, 73.87

dx.doi.org/10.1021/ic401395d | *Inorg. Chem.* 2014, 53, 2381−2395

(73.99); H, 4.13 (4.26) N, 8.20 (8.11)%. UV−visible (CH_2Cl_2) [λ_{max}, nm (ε, M^{-1} cm^{-1})]: 425, 561, 601.^{1}H NMR ($CDCl_3$, 295 K): 8.95 (*d*, 4H, *β-H*); 8.82 (*d*, 4H, *β-H*); 8.78 (*m*, 8H, *β-H*); 8.25 (*d*, 4H, Ph(por)-*H*); 8.09−8.06 (*m*, 12H, Ph(por)-*H*); 7.78 (*d*, 4H, Ph(por)-*H*); 7.73−7.61 (*m*, 18H, Ph(por)-*H*); 6.87 (*m*, 4H, Ph-*H*, DPEApy); 6.81 (*m*, 2H, Ph-*H*, DPEApy); 6.51 (*d*, 4H, Ph-*H*, DPEApy); 6.14 (*br*, 2H, N*H*, DPEApy); 5.47 (*br*, 4H, Py-*H*, DPEApy); 5.33 (*s*, 2H, Fc-*H*); 5.31 (*s*, 2H, Fc-*H*); 4.82 (*s*, 2H, Fc-*H*); 4.77 (*s*, 2H, Fc-*H*); 4.52 (*br*, 2H, C*H*, DPEApy); 2.60 (*br*, 4H, Py-*H*, DPEApy) ppm. ^{13}C NMR ($CDCl_3$, 295K): 169.37 (2C, ester-*C*); 164.03 (2C, amide-*C*); 150.60 (2C, *C*4′); 150.09−150.04 (16C, *α-C*); 144.02 (4C, *C*1′L); 143.99−143.20 (6C, *C*1); 140.74 (2C, *C*1′); 139.79 (2C, *C*3′L); 136.75 (2C, *C*1L); 135.61 (4C, *C*2′); 134.62 (12C, *C*2); 131.93−131.83 (16C, *β-C*); 128.58 (4C, *C*3L); 128.09 (2C, *C*4L); 127.33 (6C, *C*4); 126.75 (4C, *C*2L); 126.43 (12C, *C*3); 120.82, 119.70 (8C, *meso-C*); 119.80 (4C, *C*3′); 119.35 (4C, *C*2′L); 73.47 (2C, Fc-*C*2); 73.33 (2C, Fc-*C*2′); 72.97 (2C, Fc-*C*1′); 72.72 (2C, Fc-*C*3); 72.69 (2C, Fc-*C*3′); 59.26 (2C, *C*5L) ppm.

Synthesis of ***1***·*CHDApy*$_{(S,S)}$. Yield: 52 mg (87%). M. P.: > 300 °C, ESI-MS: *m*/*z* 1948.4506 ([M+2H]$^+$). Anal. Calcd (Found): C, 72.66 (72.55); H, 4.24 (4.33) N, 8.62 (8.76)%. UV−visible (CH_2Cl_2) [λ_{max}, nm (ε, M^{-1} cm^{-1})]: 425, 561, 601 . ^{1}H NMR ($CDCl_3$, 295K): 8.95 (*d*, 4H, *β-H*); 8.84 (*d*, 4H, *β-H*); 8.79−8.76 (*m*, 8H, *β-H*); 8.23 (*d*, 4H, Ph(por)-*H*); 8.13−8.06 (*m*, 12H, Ph(por)-*H*); 7.81 (*d*, 4H, Ph(por)-*H*); 7.76−7.63 (*m*, 18H, Ph(por)-*H*); 5.74 (*br*, 4H, Py-*H*, CHDApy); 5.55 (*br*, 2H, N*H*, CHDApy); 5.32 (*s*, 2H, Fc-*H*); 5.30 (*s*, 2H, Fc-*H*); 4.83 (*s*, 2H, Fc-*H*); 4.75 (*s*, 2H, Fc-*H*); 3.55 (*br*, 2H, CHDApy); 3.09 (*br*, 4H, Py-*H*, CHDApy); 1.52 (*br*, 2H, CHDApy); 1.47 (*br*, 2H, CHDApy); 0.95 (*br*, 2H, CHDApy); 0.76 (*br*, 2H, CHDApy) ppm. ^{13}C NMR ($CDCl_3$, 295K): 169.31 (2C, ester-*C*); 163.86 (2C, amide-*C*); 150.63 (2C, *C*4′); 150.11−149.95 (16C, *α-C*); 143.96 (4C, *C*1′L); 143.36 (6C, *C*1); 140.77 (2C, *C*1′); 140.14 (2C, *C*3′L); 135.65 (4C, *C*2′); 134.63 (12C, *C*2); 131.90−131.75 (16C, *β-C*); 127.33 (6C, *C*4); 126.40 (12C, *C*3); 120.73, 119.78 (8C, *meso-C*); 119.57 (4C, *C*3′); 119.24 (4C, *C*2′L); 73.35 (2C, Fc-*C*2); 73.12 (4C, Fc-*C*2′, *C*1); 72.83 (2C, Fc-*C*3); 72.67 (2C, Fc-*C*3′); 53.75 (2C, *C*1L); 31.41 (2C, *C*2L); 23.99 (2C, *C*3L) ppm.

Instrumentation. Elemental (C, H, and N) analyses were performed on a CE-440 elemental analyzer. NMR spectra were recorded on a JEOL 500 MHz instrument. The residual resonance of the solvents was used as a secondary reference. The numbering schemes used for the NMR assignments are shown in the inset of each figure. UV−visible and CD-spectra were recorded on a Perkin-Elmer UV−visible (Lambda 25) and a JASCO J-815 spectrometer, respectively. ESI-MS spectra were recorded on a waters Micromass Quattro Microtriple quadrapole mass spectrometer.

Computational Details. DFT calculations were performed at two different levels, B3LYP/6-31G** and B3LYP/LANL2DZ level. For molecule **1**, geometry optimization was carried out by employing a B3LYP hybrid functional using the Gaussian 03, revision B.04, package.[16] The method used was Becke's three parameter hybrid exchange functional,[17] the nonlocal correlation provided by the Lee, Yang, and Parr expression, and the Vosko, Wilk, and Nusair 1980 correlation functional (III) for local correction.[18] The basis set was 6-31G** for Zn, Fe, C, N, O, and H, whereas the geometry optimization of molecule **1**·DPEApy$_{(R,R)}$ was done by B3LYP/LANL2DZ. The LANL2DZ basis set uses the effective-core potential of Hay and Wadt.[19,20]

X-ray Structure Solution and Refinement. A suitable crystal of H_4FcTPP was coated with light hydrocarbon oil and mounted in the 100 K dinitrogen stream of Bruker SMART APEX CCD diffractometer equipped with CRYO Industries low-temperature apparatus, and intensity data were collected using graphite-monochromated Mo Kα radiation (λ = 0.71073 Å). The data integration and reduction were processed with SAINT software.[21] An absorption correction was applied.[22] Structure was solved by the direct method using SHELXS-97 and was refined on F^2 by full-matrix least-squares technique using the SHELXL-97 program package.[23] Non-hydrogen atoms were refined anisotropically. In the refinement, hydrogens were treated as riding atoms using SHELXL default parameters. In the structure, several highly disordered CH_2Cl_2 were present, which could not be modeled successfully and, therefore, SQUEEZE[24] was used. The overall quality of the data is poor due to weakly diffracting crystals.

■ ASSOCIATED CONTENT

Ⓢ Supporting Information

UV−visible spectral change of **1** with (1*S*,2*S*)-CHDA (Supporting Information, Figure S1), 2-aminobutane (Supporting Information, Figure S2), (1*S*,2*S*)-CHDApy (Supporting Information, Figure S3), and pyridine (Supporting Information, Figure S4); ESI-MS (Figures S5 and S6); molecular packing of H_4FcTPP (Supporting Information, Figure S7), ^{1}H−^{1}H COSY (Figures S8−S11); ^{13}C NMR (Figures S12−S18); binding constant determination (Figures S19−S22); ^{1}H NMR (Supporting Information, Figure S23) and CD and UV−visible (Supporting Information, Figure S24) of ZnTPP after addition of 1 equiv of (1*S*,2*S*)-CHDA; ^{1}H NMR of H_4FcTPP (Supporting Information, Figure S25). X-ray crystallographic details in CIF format. This material is available free of charge via the Internet at http://pubs.acs.org.

■ AUTHOR INFORMATION

Corresponding Author

*E-mail: sprath@iitk.ac.in. Phone: (+91)-512-2597251. Fax: (+91)-512-2597436.

Notes

The authors declare no competing financial interest.

■ ACKNOWLEDGMENTS

The authors thank Department of Science and Technology, Government of India, and CSIR, New Delhi for financial support. S.B., S.A.I., and A.D. thank CSIR, India for their fellowships. We thank Mr. Soumyajit Dey, Mr. Pritam Mondal, and Mr. Debangsu Sil for their help at the initial stage.

■ DEDICATION

Dedicated to Professor A. R. Chakravarty on the occasion of his 60th birthday.

■ REFERENCES

(1) (a) Berova, N.; Pescitelli, G.; Petrovica, A. G.; Proni, G. *Chem. Commun.* **2009**, 5958. (b) Hembury, G. A.; Borovkov, V. V.; Inoue, Y. *Chem. Rev.* **2008**, *108*, 1. (c) Berova, N.; Bari, L. D.; Pescitelli, G. *Chem. Soc. Rev.* **2007**, *36*, 914. (d) Borovkov, V. V.; Inoue, Y. *Top. Curr. Chem.* **2006**, *265*, 89. (e) Borovkov, V. V.; Hembury, G. A.; Inoue, Y. *Acc. Chem. Res.* **2004**, *37*, 449.

(2) (a) Brahma, S.; Asif, S. K.; Dey, S.; Rath, S. P. *Chem. Commun.* **2012**, *48*, 4070. (b) Brahma, S.; Asif, S. K.; Rath, S. P. *Inorg. Chem.* **2014**, *53*, 49.

(3) (a) Pintre, I. C.; Pierrefixe, S.; Hamilton, A.; Valderrey, V.; Bo, C.; Ballester, P. *Inorg. Chem.* **2012**, *51*, 4620. (b) Etxebarria, J.; Vidal-Ferran, A.; Ballester, P. *Chem. Commun.* **2008**, 5939.

(4) (a) Petrovic, A. G.; Vantomme, G.; Abril, Y. L. N.; Lubian, E.; Saielli, G.; Menegazzo, I.; Cordero, R.; Proni, G.; Nakanishi, K.; Carofiglio, T.; Berova, N. *Chirality* **2011**, *23*, 808. (b) Chen, Y.; Petrovic, A. G.; Roje, M.; Pescitelli, G.; Kayser, M. M.; Yang, Y.; Berova, N.; Proni, G. *Chirality* **2010**, *22*, 140. (c) Petrovic, A. G.; Chen, Y.; Pescitelli, G.; Berova, N.; Proni, G. *Chirality* **2010**, *22*, 129. (d) Kurtàn, T.; Nesnas, N.; Koehn, F. E.; Li, Y.-Q.; Nakanishi, K.; Berova, N. *J. Am. Chem. Soc.* **2001**, *123*, 5974.

(5) (a) Borovkov, V. V.; Fujii, I.; Muranaka, A.; Hembury, G. A.; Tanaka, T.; Ceulemans, A.; Kobayashi, N.; Inoue, Y. *Angew. Chem., Int. Ed.* **2004**, *43*, 5481. (b) Borovkov, V. V.; Lintuluoto, J. M.; Hembury, G. A.; Sugiura, M.; Arakawa, R.; Inoue, Y. *J. Org. Chem.* **2003**, *68*, 7176.

(c) Borovkov, V. V.; Lintuluoto, J. M.; Sugiura, M.; Inoue, Y.; Kuroda, R. *J. Am. Chem. Soc.* **2002**, *124*, 11282.
(6) (a) Tanasova, M.; Borhan, B. *Eur. J. Org. Chem.* **2012**, 3261. (b) Li, X.; Burrell, C. E.; Staples, R. J.; Borhan, B. *J. Am. Chem. Soc.* **2012**, *134*, 9026. (c) Tanasova, M.; Vasileiou, C.; Olumolade, O. O.; Borhan, B. *Chirality* **2009**, *21*, 374. (d) Li, X.; Borhan, B. *J. Am. Chem. Soc.* **2008**, *130*, 16126. (e) Li, X.; Tanasova, M.; Vasileiou, C.; Borhan, B. *J. Am. Chem. Soc.* **2008**, *130*, 1885.
(7) (a) Kai, H.; Nara, S.; Kinbara, K.; Aida, T. *J. Am. Chem. Soc.* **2008**, *130*, 6725. (b) Mizuno, Y.; Alam, M. A.; Tsuda, A.; Kinbara, K.; Yamaguchi, K.; Aida, T. *Angew. Chem., Int. Ed.* **2006**, *45*, 3786. (c) Guo, Y.-M.; Oike, H.; Saeki, N.; Aida, T. *Angew. Chem., Int. Ed.* **2004**, *43*, 4915.
(8) (a) Hayashi, T.; Aya, T.; Nonoguchi, M.; Mizutani, T.; Hisaeda, Y.; Kitagawa, S.; Ogoshi, H. *Tetrahedron* **2002**, *58*, 2803. (b) Hayashi, T.; Nonoguchi, M.; Aya, T.; Ogoshi, H. *Tetrahedron Lett.* **1997**, *38*, 1603.
(9) (a) Ishii, Y.; Yoshizawa, T.; Kubo, Y. *Org. Biomol. Chem.* **2007**, *5*, 1210. (b) Ishii, Y.; Onda, Y.; Kubo, Y. *Tetrahedron Lett.* **2006**, *47*, 8221.
(10) (a) Bringmann, G.; Götz, D. C. G.; Gulder, T. A. M.; Gehrke, T. H.; Bruhn, T.; Kupfer, T.; Radacki, K.; Braunschweig, H.; Heckmann, A.; Lambert, C. *J. Am. Chem. Soc.* **2008**, *130*, 17812. (b) Hou, J.-L.; Yi, H.-P.; Shao, X.-B.; Li, C.; Wu, Z.-Q.; Jiang, X.-K.; Wu, L.-Z.; Tung, C.-H.; Li, Z.-T. *Angew. Chem., Int. Ed.* **2006**, *45*, 796. (c) Yoon, H.; Lee, C.-H.; Jang, W.-D. *Chem.—Eur. J.* **2012**, *18*, 12479.
(11) (a) Beletskaya, I.; Tyurin, V. S.; Tsivadze, A. Y.; Guilard, R.; Stern, C. *Chem. Rev.* **2009**, *109*, 1659. (b) Harvey, P. D.; Stern, C.; Gros, C. P.; Guilard, R. *Coord. Chem. Rev.* **2007**, *251*, 401. (c) Rosenthal, J.; Nocera, D. G. *Acc. Chem. Res.* **2007**, *40*, 543. (d) Carofiglio, T.; Lubian, E.; Menegazzo, I.; Saielli, G.; Varotto, A. *J. Org. Chem.* **2009**, *74*, 9034. (e) Collman, J. P.; Wagenknecht, P. S.; Hutchison, J. E. *Angew. Chem., Int. Ed. Engl.* **1994**, *33*, 1537.
(12) (a) Iordache, A.; Oltean, M.; Milet, A.; Thomas, F.; Baptiste, B.; Aman, E. S.; Bucher, C. *J. Am. Chem. Soc.* **2012**, *134*, 2653. (b) Zhang, D.; Zhang, Q.; Su, J.; Tian, H. *Chem. Commun.* **2009**, 1700. (c) Braga, D.; Grepioni, F.; Polito, M. *Organometallics* **2006**, *25*, 4627. (d) Braga, D.; Maini, L.; Grepioni, F.; De Cian, A.; Felix, O.; Fischer, J.; Hosseini, M. W. *New J. Chem.* **2000**, *24*, 547. (e) Palekik, G. J. *Inorg. Chem.* **1969**, *8*, 2744.
(13) Beer, P. D.; Kurek, S. S. *J. Organomet. Chem.* **1987**, *336*, C17.
(14) (a) Khavasi, H. R.; Sadegh, B. M. M. *Cryst. Growth Des.* **2012**, *12*, 4798. (b) Chen, H.; An, H.; Liu, X.; Wang, H.; Chen, Z.; Zhang, H.; Hu, Y. *Inorg. Chem. Commun.* **2012**, *21*, 65.
(15) (a) www.hyperquad.co.uk/HypSpec.htm. (b) Gans, P.; Sabatini, A.; Vacca, A. *Talanta* **1996**, *43*, 1739.
(16) Frisch, M. J.; Trucks, G. W.; Schlegel, H. B.; Scuseria, G. E.; Robb, M. A.; Cheeseman, J. R.; Montgomery, J. A. J; Vreven, T.; Kudin, K. N.; Burant, J. C.; Millam, J. M.; Iyengar, S. S.; Tomasi, J.; Barone, V.; Mennucci, B.; Cossi, M.; Scalmani, G.; Rega, N.; Petersson, G. A.; Nakatsuji, H.; Hada, M.; Ehara, M.; Toyota, K.; Fukuda, R.; Hasegawa, J.; Ishida, M.; Nakajima, T.; Honda, Y.; Kitao, O.; Nakai, H.; Klene, M.; Li, X.; Knox, J. E.; Hratchian, H. P.; Cross, J. B.; Bakken, V.; Adamo, C.; Jaramillo, J.; Gomperts, R.; Stratmann, R. E.; Yazyev, O.; Austin, A. J.; Cammi, R.; Pomelli, C.; Ochterski, J. W.; Ayala, P. Y.; Morokuma, K.; Voth, G. A.; Salvador, P.; Dannenberg, J. J.; Zakrzewski, V. G.; Dapprich, S.; Daniels, A. D.; Strain, M. C.; Farkas, O.; Malick, D. K.; Rabuck, A. D.; Raghavachari, K.; Foresman, J. B.; Ortiz, J. V.; Cui, Q.; Baboul, A. G.; Clifford, S.; Cioslowski, J.; Stefanov, B. B.; Liu, G.; Liashenko, A.; Piskorz, P.; Komaromi, L.; Martin, R. L.; Fox, D. J.; Keith, T.; Al-Laham, M. A.; Peng, C. Y.; Nanayakkara, A.; Challacombe, M.; Gill, P. M. W.; Johnson, B.; Chen, W.; Wong, M. W.; Gonzalez, C.; Pople, J. A. *Gaussian 03*, Revision B.04; Gaussian, Inc.: Pittsburgh, PA, 2003.
(17) Becke, A. D. *J. Chem. Phys.* **1993**, *98*, 5648.
(18) Lee, C.; Yang, W.; Parr, R. G. *Phys. Rev. B.* **1988**, *37*, 785.
(19) Hehre, W. J.; Radom, L.; Schleyer, P. v. R.; Pople, J. A. *Ab Initio Molecular Orbital Theory;* Wiley: New York, 1986.
(20) (a) Hay, P. J.; Wadt, W. R. *J. Chem. Phys.* **1985**, *82*, 270. (b) Wadt, W. R.; Hay, P. J. *J. Chem. Phys.* **1985**, *82*, 284. (c) Hay, P. J.; Wadt, W. R. *J. Chem. Phys.* **1985**, *82*, 299.
(21) *SAINT+, 6.02 ed.;* Bruker AXS, Madison, WI, 1999.
(22) Sheldrick, G. M. SADABS 2.0, 2000.
(23) Sheldrick, G. M. *Acta Crystallogr., Sect. A* **2008**, *64*, 112.
(24) Spek, A. L. *J. Appl. Crystallogr.* **2003**, *36*, 7.